Nature Communications

https://doi.org/10.1038/s41467-026-71581-y

Article in Press

Leucine catabolic enzyme AUH regulates BAT thermogenesis via PPARγ HMGylation and RNA-binding function in male mice

Received: 31 January 2025

Accepted: 25 March 2026

Cite this article as: Jiang, H., Ni, S., Li, Z. *et al.* Leucine catabolic enzyme AUH regulates BAT thermogenesis via PPARγ HMGylation and RNA-binding function in male mice. *Nat Commun* (2026). https://doi.org/10.1038/s41467-026-71581-y

Haizhou Jiang 江海宙, Shihong Ni 倪世 , Zi Li 李紫, Shanghai Chen 上海, Xiaoying Li 李小英, Huijie Zhang 惠杰, Wei L. Shen 沈 , Xiaoxue Jiang 蒋 雪, Peixiang Luo 佩祥, Yousheng Shu 舒友生, Feixiang Yuan 原 翔, Kexin Tong 童可欣, Fei Xiao 肖斐 & Feifan Guo 郭非凡

Leucine catabolic enzyme AUH regulates BAT thermogenesis via PPARγ HMGylation and RNA-binding function in male mice

Haizhou Jiang (江海宙)[1,2], Shihong Ni (倪世鸿)[2], Zi Li (李紫)[3], Shanghai Chen (陈上海)[2], Xiaoying Li (李小英)[1], Huijie Zhang (张惠杰)[1], Wei L. Shen (沈伟)[4], Xiaoxue Jiang (蒋晓雪)[2], Peixiang Luo (罗佩祥)[2], Yousheng Shu (舒友生)[2], Feixiang Yuan (原飞翔)[2], Kexin Tong (童可欣)[2], Fei Xiao (肖斐)[1,2]* and Feifan Guo (郭非凡)[1,2]*

[1]Department of Endocrinology and Metabolism, Zhongshan Hospital, Fudan University, Shanghai, 200032, China;

[2]Institute for Translational Brain Research, State Key Laboratory of Brain Function and Disorders, MOE Frontiers Center for Brain Science, Fudan University, Shanghai, 200032, China;

[3]Shanghai Institute of Nutrition and Health, Chinese Academy of Sciences, Shanghai, 200031, China;

[4]School of Life Science and Technology, Shanghai Clinical Research and Trial Center, ShanghaiTech University, Shanghai, 201210, China.

* Correspondence: ffguo@fudan.edu.cn (Feifan Guo), xiao_fei@fudan.edu.cn (Fei Xiao)

Address: 131 Dong An Road, Shanghai, China 200032

Tel: 0086 21 54237056

Abstract

A strong association between leucine and obesity has been well established; however, the role of leucine catabolic enzymes in adipose tissue remains largely unknown. Here, we show that knockdown of the leucine catabolic enzyme AU RNA binding methylglutaconyl-CoA hydratase (AUH) in brown adipocytes reduces thermogenesis, while AUH over-expression has the opposite effect both in vivo and in vitro. Mechanistically, AUH partially promotes uncoupling protein 1 (UCP1) expression through its metabolite 3-hydroxy-3-methylglutaryl coenzyme A (HMG-CoA). HMG-CoA directly HMGylates peroxisome proliferator-activated receptor gamma (PPARγ) on lysine 386, enhancing its transcriptional activity to increase UCP1 expression. In addition, AUH binds to and stabilizes *Ucp1* mRNA via its RNA-binding function. Moreover, we discover that AUH promotes white adipose tissue browning; *AUH* expression in human white adipose tissue is inversely correlated with adiposity, and over-expression of AUH in adipose tissue protects male mice against high-fat diet-induced obesity. Collectively, these results provide new insights into the crosstalk between amino acid metabolism and thermogenesis and identify a novel post-translational modification of PPARγ.

Introduction

Obesity is now a global public health issue. The fundamental cause of obesity is an imbalance between energy intake and expenditure. Brown adipose tissue (BAT) is the main site of non-shivering

thermogenesis, which is primarily mediated by uncoupling protein 1 (UCP1). Stimulating BAT activity can improve metabolic health and is considered a promising therapeutic strategy against obesity [1].

Branched-chain amino acids (BCAAs), including leucine (Leu), isoleucine, and valine, are essential amino acids with aliphatic side chains. Many reports have shown that elevated circulating BCAA levels are associated with obesity in humans [2,3], and that decreased BCAA consumption reduces fat mass and body weight in animal models [4]. BCAAs, particularly Leu, have been linked to BAT thermogenesis [5,6]. For example, cold-induced changes in the serum levels of Leu and valine, but not isoleucine, are significantly inversely correlated with BAT activity in human subjects [5]. Following cold exposure, there is a robust increase of Leu uptake in the BAT of mice, and a modest increase in their white adipose tissue (WAT), but not in their muscle, brain, liver or heart [5]. Leu catabolic enzymes are also induced by cold exposure in the BAT of both humans and mice [5]. However, the role of Leu catabolic enzymes in thermogenesis and the underlying mechanisms remain unclear.

The first two steps of BCAA degradation are catalyzed by BCAA transaminase (BCAT) and branched-chain α–keto acid dehydrogenase complex (BCKDH), after which BCAA metabolism diverges into separate pathways. Methylcrotonoyl-CoA carboxylase (MCCC), isovaleryl-CoA dehydrogenase (IVD), and AU RNA binding methylglutaconyl-CoA hydratase (AUH) are the three key enzymes in the Leu metabolic pathway [7,8]. IVD catalyzes the conversion of isovaleryl-CoA into 3-methylcrotonyl-CoA. 3-methylcrotonyl-CoA is then metabolized into 3- methylglutaconyl-CoA (3-MG-CoA) by MCCC [7,8]. AUH is a bifunctional protein with hydratase and RNA-binding activities [9,10]. It is a methylglutaconyl-CoA hydratase that converts 3-MG-CoA into 3-hydroxy-3-methylglutaryl-CoA (HMG-CoA). AUH also binds to AU-rich elements (AREs), which are involved in directing RNA to rapid degradation. These

enzymes are involved in various physiological and pathological processes. BCAT knockout increases UCP1 expression in the BAT of mice fed on a high-fat diet (HFD) [11], while BAT-specific BCKDH knockout mice display lower core body temperature after cold exposure [5]. Considering these studies, the functions of these unique Leu-catabolic enzymes in BAT thermogenesis remain elusive.

Heat production in BAT is primarily driven by UCP1, although other contributing mechanisms exist. Over the last decades, numerous transcriptional and epigenetic regulators of UCP1 expression have been identified. Peroxisome proliferator-activated receptor gamma (PPARγ) is a central transcription factor governing many target genes in metabolic homeostasis [12,13]. Brown adipocytes have high expression of PPARγ, and PPARγ exerts critical roles in maintenance of brown adipocyte thermogenic capacity [12,13]. For example, PPARγ targets genes in BAT encoding thermogenic proteins such as UCP1 [13]. Brown adipocytes-specific knockout of PPARγ results in impaired thermogenesis in BAT [14]. PPARγ binds to a specific DNA sequence, the PPAR response element (PPRE), in the promoter region of target genes and regulates transcription. Its activity and functions are modulated by various post-translational modifications (PTMs), including phosphorylation, SUMOylation, acetylation, ubiquitination, and o-GlcNAcylation [12,15]. Many metabolites are shown to regulate thermogenesis. It's unclear whether PPARγ could be modified by some metabolites. It's intriguing and necessary to identify other PTMs of PPARγ and their related functions in adipocytes.

On the other hand, UCP1 expression is regulated at post-transcriptional level. RNA-binding proteins (RBPs) play a key role in post-transcriptional regulation. To date, a small number of RBPs, including insulin-like growth factor 2 mRNA-binding protein 2 (IGF2BP2/IMP2) and BRF1, have been shown to

affect *Ucp1* mRNA translation or stability, thereby influencing thermogenesis [16,17]. Despite these findings, the functions of most RBPs in adipocytes are unclear.

In the current study, the Leu-catabolic enzyme AUH was found to influence thermogenesis both in vitro and in vivo. Mechanistically, AUH promoted thermogenic capacity, in part by enhancing UCP1 expression through dual pathways: 1) its metabolite HMG-CoA HMGylated PPARγ to augment the transcription of *Ucp1*, and 2) its RNA-binding activity stabilized *Ucp1* mRNA. Beyond its role in brown fat, we discovered that AUH promoted WAT browning; *AUH* expression was reduced in the WAT of people with obesity and a mouse model of obesity, and AUH over-expression in adipose tissue protected mice against diet-induced obesity. Taken together, these results extend our understanding of the communication between amino acid metabolism and thermogenesis via a novel PTMs of PPARγ and demonstrate a new mechanism for the post-transcriptional regulation of *Ucp1* expression.

Results

AUH regulates brown fat UCP1 expression in vitro and in vivo

It has been reported that cold exposure induces Leu uptake and expression of Leu catabolic enzymes in BAT [5,18]. These results indicate that Leu catabolic enzymes may play a role in brown fat thermogenesis. Then we investigated the effects of these enzymes by knocking down their expression in primary brown adipocytes. The UCP1 expression and oxygen consumption rate (OCR) decreased in cells transfected with *Auh* siRNA (Fig. 1a-c and Supplementary Fig. S1a), but not in those transfected with *Ivd*, *Mccc1* or *Mccc2* siRNA (Supplementary Fig. S2a-f). Consistently, UCP1 expression and OCR were higher in primary brown adipocytes infected with adenoviruses expressing AUH (Ad-AUH) than in those infected with adenoviruses expressing green fluorescent protein (Ad-GFP) (Fig. 1d-f and Supplementary Fig. S1b).

These observations promoted us to explore the possible involvement of AUH in BAT thermogenesis in further research.

The BAT of male wild type (WT) mice was injected with adeno-associated viruses (AAV) 8 expressing short-hairpin RNA against AUH (AAV-shAUH) or a scrambled sequence (AAV-scramble). AAV-shAUH decreased AUH and UCP1 expression, as well as the OCR in BAT at room temperature (Fig. 2a-c). Whole-body oxygen consumption also decreased in the AAV-shAUH mice stimulated with or without CL316,243 injection at room temperature, a β3-AR agonist used for pharmacologic activation of thermogenesis[19] (Fig. 2d, e). The CL316,243-induced rise in oxygen consumption showed a non-significant trend toward attenuation in AAV-shAUH mice compared to controls (Fig. 2e). No differences in food intake, locomotor activity, or body weight were observed between the AAV-shAUH and control mice (Supplementary Fig. S3a-c). WAT and liver weights were not altered, while BAT weight decreased in the AAV-shAUH mice (Supplementary Fig. S3d). Although AAV-shAUH had no significant effect on the body temperature of mice at room temperature (Fig. 2f), it hampered the ability to maintain body temperature during cold exposure (Fig. 2g).

To further assess the function of AUH in BAT, we generated mice with ablation of AUH in BAT by crossing $Auh^{flox/flox}$ mice with Ucp1-Cre lines (AUH-UKO, Fig. 3b and Supplementary Fig. S4a). BAT-specific knockout of AUH did not alter BAT morphology, as assessed by H&E staining (Supplementary Fig. S4b, c). However, it reduced thermogenesis, evidenced by decreased UCP1 expression, lower BAT OCR, and reduced whole-body oxygen consumption both with and without CL316,243 injection at room temperature (Fig. 3a-e). Notably, AUH-UKO mice exhibited a significant attenuation in the CL316,243-induced rise in oxygen consumption compared to controls (Fig. 3e). There were no differences in food intake, body weight, or locomotor activity between AUH-UKO and control mice (Supplementary Fig. S4d-f). Although AUH-UKO and control mice displayed similar body temperature at room temperature (Fig. 3f), the body temperature of AUH-UKO mice was lower upon cold exposure (Fig. 3g). The UCP1

expression and OCR in BAT were lower in the AUH-UKO mice than in the control mice under cold exposure (Supplementary Fig. S4g, h).

Next, we investigated whether AUH overexpression in BAT would have the opposite effects in male WT mice infected with AAV8 expressing AUH (AAV-AUH) or control GFP (AAV-GFP). AUH overexpression increased UCP1 expression and OCR in BAT at room temperature (Fig. 4a-c). Whole-body oxygen consumption also increased in AAV-AUH mice at room temperature in the absence of any changes in locomotor activity (Fig. 4d and Supplementary Fig. S5a). In addition, AAV-AUH increased mice body temperature at room temperature and improved their ability to maintain body temperature following cold exposure (Fig. 4e, f). Moreover, AUH overexpression in BAT decreased fat mass, as measured by nuclear magnetic resonance (Fig. 4g). WAT weight decreased and BAT weight increased in AAV-AUH mice (Supplementary Fig. S5b). Although the body weight of AAV-AUH mice appeared to be slightly reduced, the difference between the AAV-AUH mice and control mice was not statistically significant (Supplementary Fig. S5c).

To confirm the role of UCP1 in the AUH-mediated effects, WT and UCP1 null (*Ucp1*$^{-/-}$) mice were infected with AAV-AUH or AAV-GFP. WT mice infected with AAV-AUH displayed significantly higher body temperature at room temperature and under cold conditions, as well as higher whole-body oxygen consumption at room temperature (Supplementary Fig. S6a-c). However, these effects were attenuated in *Ucp1*$^{-/-}$mice (Supplementary Fig. S6a-c). Similarly, UCP1 knockdown in BAT by injection of AAV-shUCP1 attenuated the AAV-AUH-induced increases in body temperature at room temperature and under cold conditions (Supplementary Fig. S6d, e). The increase in isoproterenol-stimulated respiration induced by AUH overexpression was abolished when UCP1 was knocked down in primary brown adipocytes (Supplementary Fig. S6f). These results support a role for UCP1 in AUH-regulated thermogenesis and body temperature.

HMG-CoA contributes to the effects of AUH on UCP1 expression

Since AUH catalyzes the hydration of 3-MG-CoA to HMG-CoA, we were promoted to investigate the possible involvement of the metabolite in AUH function. As expected, HMG-CoA levels were significantly reduced in the BAT of AAV-shAUH mice (Fig. 5a). Similarly, other metabolites derived from products downstream of AUH, including acetoacetate and acetyl-CoA, were decreased in the BAT of AAV-shAUH mice compared to those in control mice (Supplementary Fig. S7a). In contrast, AUH knockdown in BAT resulted in the accumulation of α-KIC, isovaleryl-CoA, and 3-methylcrotonyl-CoA (Supplementary Fig. S7a). HMG-CoA levels were also reduced in the BAT of AUH-UKO mice compared to $AUH^{flox/flox}$ controls (Supplementary Fig. S7b). Interestingly, in control ($AUH^{flox/flox}$) mice, cold stress increased HMG-CoA levels in BAT. However, this cold-adaptive response was attenuated in AUH-UKO mice (Supplementary Fig. S7b).

We then focused on the product of AUH and found that supplementation with HMG-CoA increased AUH knockdown-reduced UCP1 expression in primary brown adipocytes (Fig. 5b, c and Supplementary Fig. S7d). Additionally, in AUH-UKO mice, HMG-CoA administration rescued the knockout-induced deficits: it restored UCP1 expression in BAT, basal and CL316,243-stimulated whole-body oxygen consumption, and body temperature during cold exposure (Supplementary Fig. S8a-d). These results demonstrate that HMG-CoA contributes to the regulation of UCP1 expression, and that HMG-CoA supplementation rescues the impaired thermogenesis caused by AUH deficiency in vivo. However, this rescue likely involves both the rapid substrate-provision role of HMG-CoA (evidenced by acute recovery of oxygen consumption) and its slower, HMGylation-dependent transcriptional effects (as discussed later).

Next, we investigated the effects of AUH on the expression of several transcriptional regulators of UCP1, including PPARγ, PR domain-containing protein 16 (PRDM16), and PPARγ co-activator 1 alpha (PGC-1α). However, the expression levels of PPARγ, PRDM16 and PGC-1α were not changed in the BAT of AAV-shAUH or AAV-AUH mice (Fig. 5d, e). PRDM16 and PGC-1α bind to PPARγ and activate its transcriptional function to regulate UCP1 expression. Therefore, we assessed the effects of AUH on PPARγ transcriptional activity using the PPRE luciferase reporter assay system and a PPARγ Transcription Factor Assay Kit. AUH knockdown reduced the transcriptional activity of PPARγ in primary brown adipocytes, and this was rescued by HMG-CoA supplementation (Fig. 5f, g). Consistently, AUH knockdown decreased the binding of PPARγ to the *Ucp1* promoter in primary brown adipocytes, and this was also rescued by HMG-CoA supplementation, as demonstrated by a chromatin immunoprecipitation (ChIP) assay (Fig. 5h). We then explored the possible involvement of PPARγ in AUH-regulated UCP1 expression, and observed that PPARγ over-expression blocked the AUH knockdown-induced reductions in UCP1 expression in primary brown adipocytes (Fig. 5i). Taken together, these results suggest that HMG-CoA contributes to AUH-regulated UCP1 expression, at least partially via affecting PPARγ activity. Although PPARγ is important for adipocyte differentiation, neither AUH knockdown nor overexpression affected brown preadipocyte differentiation (Supplementary Fig. S9a-d).

AUH regulates the HMGylation of PPARγ via HMG-CoA

As a reactive metabolite, HMG-CoA can non-enzymatically modify proteins and affect their activity [20,21]. We therefore investigated the mechanisms by which HMGylation mediates the effects of AUH. First, we examined global protein HMGylation in BAT lysates from control and AUH-UKO mice. Western blot

analysis indicated that BAT protein HMGylation was lower in AUH-UKO mice than in control mice (Fig. 6a). Then the HMGylation of PPARγ was measured. AAV-AUH led to an increase in HMGylation of PPARγ in BAT (Fig. 6b), and AAV-shAUH had the opposite effects (Fig. 6c). PPARγ HMGylation levels were also lower in the BAT of AUH-UKO mice relative to $AUH^{flox/flox}$ controls (Supplementary Fig. S7c). Notably, cold exposure induced an increase in BAT PPARγ HMGylation in control mice, whereas this induction was attenuated in AUH-UKO mice (Supplementary Fig. S7c). In addition, AUH knockdown reduced the HMGylation of PPARγ in primary brown adipocytes (Fig. 6d), which was rescued by 0.5mM HMG-CoA supplementation (Fig. 6e). To determine whether HMG-CoA directly causes PPARγ HMGylation, purified PPARγ was incubated with 0.5 or 1 mM HMG-CoA. The incubation of purified PPARγ with HMG-CoA led to its HMGylation (Fig. 6f). Interestingly, HMG-CoA did not cause significant HMGylation of purified PRDM16 under the same conditions (Supplementary Fig. S7e). We further assessed the impact of HMGylation on PPARγ activity. Purified PPARγ was pre-incubated with 0.5mM HMG-CoA before detecting its DNA-binding activity. The addition of HMG-CoA increased the DNA binding activity of PPARγ (Fig. 6g). Moreover, we confirmed that HMG-CoA upregulated the transcriptional activity of PPARγ using the PPRE luciferase reporter assay system in HEK 293 cells (Fig. 6h). Collectively, these data indicate that AUH regulates the HMGylation of PPARγ via HMG-CoA.

To identify the potential HMGylation sites within PPARγ, we performed liquid chromatography-mass spectrometry (LC-MS/MS) analysis using purified PPARγ incubated with HMG-CoA. Nine lysine residues were detected within the 145–466 amino acid region of PPARγ protein (Fig. 7a, b). We then introduced a lysine (K)-to-arginine (R) mutation into the lysine residue of PPARγ and found that K386R mutation impaired the HMGylation and transcriptional activity of PPARγ. First, we immunoprecipitated

and purified the WT FLAG-PPARγ protein from HEK 293 cells transfected with WT FLAG-PPARγ-expressing plasmids. We performed an *in vitro* HMGylation assay and observed an increase in the HMGylation of WT FLAG-PPARγ protein after HMG-CoA incubation (Supplementary Fig. S7f). However, HMG-CoA-induced HMGylation was lower in the FLAG-PPARγ-K386R protein than in the WT FLAG-PPARγ protein (Fig. 7c). Lysine 386 is evolutionarily conserved in vertebrate PPARγ (Fig. 7d). Secondly, we examined the transcriptional activity of WT PPARγ or PPARγ-K386R using the PPRE luciferase reporter assay system in HEK 293 cells. The transcriptional activity of WT PPARγ increased after HMG-CoA treatment, but no changes were observed for the PPARγ-K386R mutant (Fig. 7e). Finally, we found that the PPARγ-K386R mutant failed to increase *Ucp1* expression as much as WT PPARγ in primary brown adipocytes treated with HMG-CoA (Fig. 7f). Together, these results demonstrate that PPARγ HMGylation on K386 impacts its transcriptional activity.

AUH binds to and stabilizes *Ucp1* mRNA

AUH is a bifunctional protein involved in Leu catabolism and RNA binding [22]. To determine if its RNA-binding activity mediates effects on UCP1 expression, we expressed mutant AUH forms in primary brown adipocytes. The A215V mutation impaired catalytic activity but not RNA-binding[10,23] (Supplementary Fig. S10a), while the K80N/K84E/K88Q mutation impaired RNA-binding but not catalysis[23] (Supplementary Fig. S10a, b). Overexpression of either mutant decreased UCP1 expression compared to wild-type AUH, indicating both catalytic and RNA-binding functions regulate UCP1 expression (Supplementary Fig. S10c). To further dissect contributions of the PPARγ pathway versus mRNA stability, we performed two assays. Treatment with a transcription inhibitor actinomycin D[17] reduced AUH-mediated UCP1 upregulation (Supplementary Fig. S10d), implicating mRNA stabilization.

Conversely, the PPARγ antagonist GW9662 attenuated, but did not abolish completely, the AUH-induced increase in *Ucp1* mRNA (Supplementary Fig. S10e), revealing a PPARγ-independent component consistent with RNA stabilization. These results indicate that AUH enhances *Ucp1* mRNA levels through both PPARγ-dependent transcription and RNA stabilization.

As an AU RNA binding protein, AUH binds to an ARE of mRNA, a sequence containing a cluster of the pentanucleotide AUUUA [9]. To understand the mechanisms of how AUH functions as an RBP here, we performed RNA immunoprecipitation sequencing (RIP-seq) to detect the mRNAs bound to AUH in BAT. Kyoto Encyclopedia of Genes and Genomes (KEGG) enrichment analysis revealed that the thermogenesis-related pathways were remarkably enriched (Fig.8a). Among the AUH-interacting RNA transcripts involved in thermogenesis, *Ucp1* is a major potential target of AUH (Fig.8a). According to the RIP-seq data, the AUH-binding sites were predominantly located in the 3′ untranslated region (3′ UTR) of *Ucp1* mRNA (Fig.8b); three AREs were also found in this region (Supplementary Fig. S10f). This suggests that AUH may regulate *Ucp1* mRNA by binding to AREs. We first examined whether AUH interacts with *Ucp1* mRNA using an RNA immunoprecipitation (RIP) assay. BAT lysates from male WT mice were immunoprecipitated with control IgG or anti-AUH antibody, and specific primers were used to identify the AREs in the 3′ UTR of *Ucp1* mRNA by quantitative real-time PCR (RT-qPCR) analysis. We found that *Ucp1* mRNA were highly enriched in anti-AUH immunoprecipitates compared to IgG controls (Fig.8c). We next conducted an RNA pull-down assay using purified AUH protein and in vitro transcribed *Ucp1* 3′ UTR mRNA fragments. As expected, the *Ucp1* 3′ UTR mRNA fragments could retrieve AUH protein (Fig.8d). Together, these results demonstrate an interaction between AUH protein and the 3′ UTR of *Ucp1* mRNA.

AREs are found in the 3′ UTR of certain mRNAs and implicated in the control of mRNA decay [24]. Therefore, we examined whether AUH affects *Ucp1* mRNA stability. Actinomycin D was used to inhibit transcription in primary brown adipocytes transfected with or without *Auh* siRNA, and the *Ucp1* mRNA

decay rate was measured. The half-life of *Ucp1* mRNA in primary brown adipocytes transfected with *Auh* siRNA was shorter than that in control cells (1.84 vs. 2.77 h, Fig.8e), while that in AUH-overexpressing cells was longer (Fig.8f). Moreover, AUH with K80N/K84E/K88Q mutation did not affect *Ucp1* mRNA stability compared to the control group (Fig.8g), whereas over-expression of the A215V mutant AUH had the same effects on *Ucp1* mRNA stability as WT AUH (Fig.8h). No differences were observed in the 18s rRNA under these conditions (Fig.8e-h). Consistent with these observations, AUH knockdown reduced the luciferase activity of *Ucp1* 3′ UTR in primary brown adipocytes, and AUH over-expression had the opposite effects (Fig.8i). Overall, these data support the role of AUH in stabilizing *Ucp1* mRNA.

Over-expression of AUH in adipose tissue protects mice against high-fat diet (HFD)-induced obesity

Given that AUH increases UCP1 expression in BAT and primary brown adipocytes, we investigated the effects of AUH on WAT browning. The subcutaneous WAT (sWAT) of male WT mice was injected with AAV-AUH or AAV-GFP. There was no difference in food intake between AAV-AUH and control mice (Supplementary Fig. S11a). UCP1 expression and OCR were higher in the sWAT of AAV-AUH mice than in control mice (Fig.9a-c). AAV-AUH decreased adipocyte size and the weight of sWAT compared to those in control mice (Fig.9d, e). Moreover, *Ucp1* mRNA levels and the OCR were higher in primary white adipocytes infected with Ad-AUH than in control cells (Fig.9f, g and Supplementary Fig. S1c). Collectively, these results suggest that AUH promotes WAT browning. Mirroring observations in BAT, AAV-AUH elevated HMG-CoA levels and PPARγ HMGylation in sWAT compared to AAV-GFP control mice (Fig. 9h, i). AUH overexpression also increased PPARγ HMGylation in primary white adipocytes (Fig. 9j).

To establish a correlation between AUH levels and obesity, we analyzed AUH expression in two

WAT mRNA expression profiles of people with obesity from the Gene Expression Omnibus (GEO) database. Analysis of these datasets showed lower *AUH* gene expression in the WAT of individuals with obesity [25,26] than in that of lean individuals (Fig.10a). In addition, we found decreases in AUH protein abundance and HMG-CoA levels in the sWAT of mice fed a HFD compared with those fed a normal chow diet (NCD, Fig.10b, c).

We further examined the anti-obesity effects of AUH in HFD-fed mice. The BAT and sWAT of male WT mice were injected with AAV-AUH or AAV-GFP. The mice were fed a HFD, and changes in their metabolic parameters were measured. AAV-AUH mice gained less body weight and fat mass than control mice under HFD conditions (Fig.10d, e), and their WAT weight was lower (Fig.10f). Food intake was comparable between the two groups (Supplementary Fig. S11b). Subsequently, we found that AAV-AUH mice showed higher *Ucp1* mRNA and protein levels in the BAT than control mice under HFD conditions (Fig.10g). AAV-AUH also increased the UCP1 expression and decreased the adipocyte size of sWAT (Fig.10h, i). AAV-AUH mice displayed higher whole-body oxygen consumption compared to controls (Supplementary Fig. S11c). However, knocking down UCP1 expression in BAT and sWAT attenuated this AUH-induced increase in oxygen consumption, demonstrating a role of UCP1 in mediating AUH's anti-obesity effects (Supplementary Fig. S11c). Furthermore, AAV-AUH mice exhibited improved insulin sensitivity and glucose tolerance under HFD conditions, although their blood glucose and serum insulin levels remained the same as those in control groups (Fig.10j and Supplementary Fig. S11d, e). These results demonstrate that AUH over-expression in adipose tissue ameliorates diet-induced obesity and insulin resistance.

Discussion

Adipose tissue is critical for maintaining energy homeostasis. The major function of BAT is to produce heat, in large part through UCP1 activation, making it a promising therapeutic target for treating obesity [27]. BCAAs, particularly Leu, are closely associated with brown fat thermogenesis [5,6]. Leu uptake and catabolic enzyme expression are induced in BAT upon cold exposure [5,18]; however, the exact role of Leu catabolic enzymes in thermogenesis remains unclear. Here, we explored the effects of unique Leu-catabolic enzymes on brown fat thermogenesis. We found that AUH knockdown reduced the OCR and UCP1 expression in primary brown adipocytes, whereas AUH overexpression had the opposite effects. These results suggest that AUH directly activates brown adipocytes. However, knockdown of IVD, MCCC1 or MCCC2 did not influence the OCR or UCP1 expression in primary brown adipocytes. These observations indicate that individual Leu-catabolic enzymes have different effects on thermogenesis. A possible reason for this may be that these catabolic enzymes harbor non-canonical functions, apart from their established roles in Leu metabolism. For example, AUH also possesses RNA-binding activity [9]. MCCC1 is shown to interact with mitochondrial antiviral signaling protein (MAVS), thus participating in innate immunity against viral infections [28]. It also interacts with sirtuin 4 (SIRT4) and may mediate its physiology [29,30]. Many MCCC2-binding proteins have been identified in tumor cells, and these proteins are enriched in protein and energy metabolism [31]. Understanding these non-canonical functions may broaden the horizon of the Leu metabolism field.

Consequently, our investigation focused on AUH. AUH was first characterized in 1995 [9], and subsequent studies have demonstrated that it is a bifunctional protein with RNA-binding activity and converts 3-MG-CoA into HMG-CoA during Leu catabolism [10,22]. AUH is highly expressed in tissues with

high energy demands [32], and has been implicated in many physiological and pathological states. Mutations in the AUH gene have been shown to cause 3-methylglutaconic aciduria type I [33,34], a disorder with the common feature of elevated 3-methylglutaconic acid levels in the urine. Additionally, the administration of some mood stabilizers can up-regulate *Auh* mRNA levels in mouse brain [35]. However, the function of AUH in brown fat thermogenesis is poorly understood. Our in vivo results were similar to those obtained in vitro. AUH knockdown inhibited brown fat thermogenesis, as demonstrated by the reduced OCR and UCP1 expression in the BAT of AAV-shAUH mice. Moreover, AUH knockdown in BAT decreased basal and CL316,243-stimulated whole-body oxygen consumption. The fact that body temperature at room temperature was not altered by AUH knockdown in BAT may be because that the body does not need to produce significant heat under basal conditions. For example, the body temperature does not differ between WT and UCP1 null mice at room temperature [36]. Consistent with this possibility, AAV-shAUH mice were unable to maintain their body temperature during acute cold exposure. Similar effects were observed in BAT specific AUH knockout mice. AUH deficiency did not cause overt developmental defects in BAT under our conditions. This aligns with Balaz et al.[37], who reported that statins inhibiting the mevalonate (MVA) pathway impaired WAT browning but did not affect brown adipocyte maturation or UCP1 levels in BAT. While Kwon et al. [38]observed BAT atrophy in models of embryonic statin exposure or brown adipocyte-specific *Hmgcr* knockout, they also reported unchanged *Ucp1* mRNA levels in the atrophied BAT of *Hmgcr* knockout mice. This dissociation between morphology and *Ucp1* expression in Kwon et al.'s model, alongside our histological data, suggests that perturbations impacting the MVA/geranylgeranyl pyrophosphate (GGPP) pathway can have context-dependent effects. Furthermore, AUH deficiency may divert HMG-CoA metabolism toward the HMGCL pathway rather than inhibiting

the MVA pathway, thus not severely impairing BAT development—unlike HMGCR inhibition (e.g., by statins). The observed downregulation of UCP1 in mature AUH-UKO BAT without morphological alterations may reflect a specific impact on the thermogenic program rather than developmental pathways, consistent with examples where UCP1 expression changes occur independently of BAT development [39]. In contrast, AUH overexpression increased UCP1 expression and OCR in BAT. Interestingly, AUH overexpression in BAT also increased whole-body oxygen consumption and body temperature at room temperature, and decreased fat mass. This is consistent with other reports that show a negative relationship between BAT activity and the body mass index [40]. These observations indicate that the Leu catabolic enzymes in BAT play important role in systemic energy metabolism.

The UCP1 is a central and well-characterized mediator of thermogenesis in BAT, although other contributing systems exist [41]. Our data showed that AUH modulated UCP1 expression at both the mRNA and protein levels, and genetic loss of UCP1 attenuated key metabolic phenotypes induced by AUH overexpression, supporting a contributory role for UCP1 in mediating AUH's effects. To elucidate how AUH impacts this key thermogenic component, we investigated the mechanisms underlying AUH-regulated UCP1 expression. Our further study demonstrated that AUH influenced *Ucp1* mRNA synthesis and degradation via different mechanisms. However, the relative importance of these two regulatory modes, and their interplay with other AUH-dependent processes (such as metabolic substrate provision), may vary with physiological context and requires further investigation.

AUH catalyzes the conversion of 3-MG-CoA to HMG-CoA. We found that AUH knockdown or knockout in BAT reduced HMG-CoA levels; however, the biological function of HMG-CoA in adipocytes remains poorly understood. The negative effects of AUH knockdown on UCP1 mRNA and protein levels

were rescued by HMG-CoA in primary brown adipocytes, suggesting that HMG-CoA directly affects UCP1 expression. Another source of HMG-CoA is cholesterol biosynthesis. During this process, HMG-CoA synthase (HMGCS) coverts acetoacetyl-CoA to HMG-CoA. In line with our observations, the inhibition of HMGCS suppresses UCP1 expression and thermogenic function in brown adipocytes [37], although whether HMG-CoA mediates HMGCS-regulated UCP1 expression remains unknown. Besides its role in up-regulating *Ucp1* expression, HMG-CoA provides substrates for the tricarboxylic acid (TCA) cycle, which is involved in energy generation and important for thermogenesis [42]. The reduction in basal respiration observed upon AUH loss is consistent with a metabolic substrate limitation. AUH deficiency lowers HMG-CoA and consequently acetyl-CoA levels, directly reducing the flux of key fuels into the TCA cycle. This diminished substrate supply likely constrains mitochondrial oxidative metabolism, thereby lowering the basal OCR. Thus, the altered basal respiration reflects a functional reprogramming of cellular energetics—primarily driven by AUH's role in maintaining the leucine catabolism-derived acetyl-CoA pool. Finally, we cannot rule out the possibility that the effect of AUH on *Ucp1* expression is, in part, due to changes in other upstream or downstream metabolites. These possibilities require to be investigated in future studies.

We further explored the mechanisms underlying HMG-CoA-regulated *Ucp1* expression. Recent studies have shown that HMG-CoA can undergo intramolecular catalysis to form a reactive intermediate capable of non-enzymatically acylation on proteins and alter their activities, such as fatty acid synthase (FAS) and malate dehydrogenase (MDH2) [20,21]. Therefore, we speculated that the effects of HMG-CoA on *Ucp1* expression might be mediated through protein HMGylation and focused on the transcriptional regulators of UCP1. Our data revealed a critical role of PPARγ here. First, changes in AUH expression or

HMG-CoA levels induced alterations in PPARγ HMGylation and its transcriptional activity. Secondly, PPARγ over-expression could rescue the inhibitory effect of AUH knockdown on *Ucp1* expression. PPARγ is a key transcription factor for brown fat thermogenesis. Many well described PTMs modulating PPARγ function have been identified, including phosphorylation on serine 112/273, SUMOylation on lysine 107/395, acetylation on lysine 98/107/218/268/293, ubiquitination on lysine 184/185, and o-GlcNAcylation on threonine 54 [12,15,43]. Our results indicate that lysine 386 of PPARγ is targeted for HMGylation by HMG-CoA. Lysine 386 is located in the C-terminal ligand-binding domain, which contains the ligand-binding pocket, regions important for dimerization, and the AF-2 domain [15]. We found that the K386R mutation decreased HMG-CoA-induced PPARγ HMGylation and activity. Further analyses of PPARγ and HMG-CoA structure are required to explain the reasons behind lysine 386 HMGylation. A previous study demonstrated that a histone deacetylase 3 (HDAC3) inhibitor can induce PPARγ acetylation at multiple lysine sites and enhance its transcriptional activity [44]. Interestingly, the authors detected lysine 386 as an acetylated site of PPARγ by mass spectrometry, but they didn't perform further experiments to support this finding, and the function of this acetylated lysine site in PPARγ is unknown. We found that the K386R mutation reduced UCP1 expression, suggesting that this residue is important for thermogenesis in adipocytes. The role of PPARγ lysine 386 HMGylation in regulating other physiological processes remains to be determined by further research. Overall, we provided evidence showing a new PTM of PPARγ here. Our findings broaden understanding of the biological functions of protein HMGylation, particularly its role in adipocyte metabolism. It would be interesting to investigate the HMGylation of other PPAR isotypes and their related functions in various tissues.

Soon after the discovery of UCP1 as a critical protein in thermogenesis, many transcriptional factors

and signaling pathways regulating *Ucp1* mRNA synthesis were studied [45]. However, the post-transcriptional mechanisms underlying *Ucp1* expression remain largely unknown. A small number of RBPs have been shown to participate in these processes, and consequently in metabolic homeostasis. For example, IGF2BP2/IMP2 inhibits *Ucp1* mRNA translation, and mice lacking IMP2 resist diet-induced obesity [16]. In contrast, cytoplasmic polyadenylation element binding protein 2 (CPEB2) activates *Ucp1* mRNA translation and promotes thermogenesis in BAT [46]. The absence of Quaking (QKI) promotes *Ucp1* mRNA nuclear export and translational efficacy but not stability, leading to brown fat activation and WAT browning [47]. BRF1 destabilizes *Ucp1* mRNA and contributes to obesity [17]. Apart from its role in Leu metabolism, AUH functions as an RBP and targets mRNAs containing AREs [9]. Our RIP-seq data revealed that many AUH-binding mRNAs were involved in thermogenesis. Further investigation demonstrated that AUH bound to the AREs in the 3′ UTR of *Ucp1*, thereby improving its mRNA stability. A similar role has previously been reported for AUH; it has been shown to bind to the AU-rich 3′ UTR of *c-fos*, *c-myc*, and *interleukin 3* in vitro [9], directing rapid decay in mRNAs. Overall, these results suggest AUH as an important post-transcriptional factor that controls adipocyte thermogenesis. Our study, along with the existing literature, highlights the importance of the post-transcriptional regulation of thermogenic gene expression and uncovers the crosstalk between RNA metabolism and thermogenesis.

White adipose tissue depots are major energy storage sites [48,49]. White fat can acquire a brown fat-like phenotype in response to a variety of stimuli such as cold. These cells are called beige cells, and this process is known as white fat browning [48,49]. The induction of white fat browning increases thermogenesis and promotes overall health [1,49]. In line with the role of AUH in increasing UCP1 expression in brown fat, we also found that AUH promoted WAT browning. Further investigation revealed a strong negative

association between AUH expression in WAT and obesity in both humans and mice. Consistently, HMG-CoA levels were reduced in the WAT of HFD-fed mice, and AUH over-expression in adipose tissue prevented HFD-induced obesity. Obesity is also associated with the development of Type 2 diabetes. We found that AUH over-expression in adipose tissue ameliorated insulin resistance in a mouse model of obesity. These results demonstrate that AUH over-expression in adipose tissue has beneficial effects on whole-body metabolic homeostasis, suggesting that AUH may be a potential target for treating obesity and associated metabolic disorders.

In summary, this study demonstrates that AUH enhances brown fat thermogenesis partially through the upregulation of UCP1, via both transcriptional and post- transcriptional mechanisms (Fig. 10k). Notably, the acute recovery of oxygen consumption upon HMG-CoA injection in AUH-KO mice suggests rapid substrate-driven effects, likely through acetyl-CoA replenishment. This acute mechanism operates in parallel to the slower, HMGylation-mediated transcriptional program, together enabling both immediate and sustained thermogenic responses. We therefore propose a synergistic model wherein AUH supports thermogenesis through dual routes: (1) by maintaining acetyl-CoA pools via leucine catabolism, and (2) by producing HMG-CoA as a precursor for PPARγ HMGylation, which in turn elevates UCP1 expression. This integrated mechanism positions AUH as a metabolic node coordinating both fuel availability and transcriptional activation of the thermogenic program.

These insights expand our understanding of the interface between amino acid metabolism and adipose tissue thermogenesis, highlighting potential targets for metabolic disease therapeutics. Individual BCAAs have specific effects on metabolic homeostasis, most likely because each BCAA is involved in a unique metabolic process. This study elucidates the mechanisms underlying these observations. Clinically,

PPARγ is a promising target for drug development; activating PPARγ using full agonists can reportedly improve insulin sensitivity and induce white fat browning, with some side effects. Mimicking or blocking PPARγ modification, instead of changing the entire signaling pathway, may be a more effective strategy that could reduce the adverse effects.

Methods

Animals

All mice experiments were conducted in accordance with the guidelines of the Institutional Animal Care and Use Committee at Fudan University (ethical committee approval no.2022030006S). Eight to ten-week-old male C57BL/6J mice were used in the study. Wild-type (WT) and Auh$^{flox/flox}$ mice were purchased from Shanghai Model Organisms (China). The *Ucp1*$^{-/-}$ and Ucp1-Cre mice were kindly provided by Prof. Xinran Ma (East China Normal University) or Prof. Jiqiu Wang (Ruijin Hospital, Shanghai Jiao Tong University School of Medicine), respectively. Mice were housed on a 12 h light/dark cycle at 24±1℃ and provided free access to standard chow rodent diets (XTI01FZ-011, Jiangsu Xietong Pharmaceutical Bio-Engineering Co., Ltd, China) and water. Mice were euthanized by CO_2 inhalation. For mice fed with HFD (60 % fat, D12492, Research Diets, USA), six-week-old C57BL/6J mice were injected with AAV-AUH or AAV-GFP, AAV-shUCP1 or AAV-scramble in BAT and sWAT for 4 weeks before fed with HFD.

Isolation of primary adipocytes, cell culture, and treatments

Mice at 4-5 weeks or 7-14 days of age were utilized for dissecting sWAT or BAT, respectively[50]. In brief, sWAT or BAT were minced and digested with Type I collagenase (Worthington, USA) in 37 ℃ water bath for about 30 min. For white adipocyte differentiation, confluent cells were cultured in DMEM

(Gibco, USA) supplemented with 10 % FBS, 0.5 mM isobutylmethyxanthine (IBMX, MCE, China), 1 μM dexamethasone (Dex, MCE, China), and 1.7 μM insulin (MCE, China) for 48 h. Then cells were cultured in DMEM with 10 % FBS and 1.7 μM insulin until harvest. For brown adipocyte differentiation, confluent cells were cultured in DMEM supplemented with 10 % FBS, 0.5 mM IBMX, 5 μM Dex, 1 nm T3 (MCE, China), 125 μM indomethacin (MCE, China), and 20 nM insulin for 48 h. Then cells were cultured in DMEM with 10 % FBS, 20 nM insulin and 1 nm T3 until harvest. Differentiated adipocytes were transfected with siRNAs or plasmids using Lipofectamine 3000 reagent (Invitrogen, USA). GW9662 (HY-16578) and actinomycin D (HY-17559) were from MCE, China. Oil Red O staining was assessed using kits (C0157S, Beyotime, China) according to the manufacturers' protocols.

Plasmids and RNA interference

The plasmids pcDNA3.0-FlAG-AUH (mouse), pcDNA3.0-FlAG-PPARγ (human), and their mutants were constructed by insertion of the corresponding cDNA into pcDNA3.0 vectors. Plasmid pGEX-4T-1-AUH, for expressing mouse AUH in *E. coli*, was constructed by inserting the corresponding cDNA into the pGEX-4T-1 vector. The plasmid expressing mouse PPARγ was kindly provided by Prof. Qunying Lei (Fudan University). The pPPARγ-Fluc-hRluc luciferase reporter was generated by cloning three PPRE into pMCS-Fluc-SV40-hRluc-Neo vectors. The luciferase-*Ucp1* 3′ UTR reporter was constructed by cloning *Ucp1* 3′ UTR into pmirGLO vectors.

siRNAs were synthesized by GenePharma (Shanghai, China). The siRNA sequences were 5′-ACGAGCCAAGATGCATTCCAGTGAA-3′ (si-*Auh*-1) and 5′-GCCATGTGTTAGAACAGAA-3′ (si-*Auh*-2) for AUH, 5′-CAATGGCCCTGATGC TGATATCCTA-3′ (si-*Ivd*-1) and 5′-CATGTGTTGGTAATGGAAGAGATAT-3′ (si-*Ivd*- 2) for IVD, 5′-CGTCTGCAATTAGAGACATGGGTAT-3′ (si-*Mccc1*-1) and 5′-GCAGATTGACAACAAGTCCTT-3′ (si-*Mccc1*-2) for MCCC1, 5′-GACAGAATCG ACAATCTCATA-3′ (si-*Mccc2*-1) and 5′-

GTGCCTAAGATAACTGTCATA-3′ (si-*Mccc2*-2) for MCCC2, 5′-UCCUGGAACGUCAUCAUGUTT-3′ for UCP1. The siRNA sequence for si-*Auh*-1 was used unless otherwise specified.

Generation and administration of viruses

Adenoviruses expressing mouse AUH (Ad-AUH-FLAG), its mutants (Ad-AUH-A215V-FLAG, Ad-AUH-K80N/K84E/K88Q-FLAG), or GFP (Ad-GFP) were purchased from Vigene Biosciences (China). The adipocytes were infected with adenoviruses at a multiplicity of infection [MOI] of 50/cell. Adeno-associated viruses (AAV) expressing mouse AUH (AAV8-CMV-AUH-FLAG), GFP (AAV8-CMV-GFP), short-hairpin RNA against AUH (AAV8-U6-shAUH) or UCP1 (AAV8-U6-shUCP1), and a scramble control were purchased from Vigene Biosciences (China). The shRNA sequence for *Auh* was 5′-GCCATGTGTTAGAACAGAA-3′, and that for *Ucp1* was 5′-GGTCCTGGAACGTCATCATGT-3′. AAV diluted in PBS were injected into the interscapular BAT or sWAT following a published protocol [11,51]. Interscapular BAT received 1×10^{12} vector genomes/ mouse AAV using a syringe. Mouse sWAT was injected on both sides, and each side received 1×10^{12} vector genomes AAV. AAV were injected into the sWAT fat pads at multiple points (10 points per fat pad). The metabolic parameters of mice infected with AAV were analyzed after 4 weeks.

Mitochondrial function and respiration

We monitored OCR using XFe24 Extracellular Flux Analyzer (Agilent Technologies, USA) according to the manufacturer instructions. Differentiated primary brown adipocytes in the culture microplates were equilibrated in XF Assay Medium (Agilent Technologies, USA) with 2 % fatty acid-free BSA, 1mM sodium pyruvate (Gibco, USA), 1 mM L-glutamine (Gibco, USA) and 10 mM glucose, pH 7.4, at 37 ℃ without CO_2 for 1 h. Then adipocytes were treated with 4 μM oligomycin (MCE, China),

0.5 μM isoproterenol (Merck, Germany), 2 μM carbonyl cyanide 4-(trifluoromethoxy) phenylhydrazone (FCCP, MCE, China), 1 μM antimycin A (ENZO, USA), and 1 μM rotenone (MCE, China)[52,53]. Total protein of each well was extracted and quantified for normalization. The OCR values were also normalized to non-mito OCR and analyzed by Wave Desktop (Agilent Technologies, USA). The ISO-induced OCR was calculated as the maximal increase in the OCR induced by isoproterenol, above the OCR level measured after oligomycin injection [54]. In addition, freshly isolated BAT (~3 mg) or sWAT (~10 mg) were used to measure the OCR. BAT was treated with 30 μM oligomycin, 10 μM FCCP, 15 μM antimycin A, and 5 μM rotenone. sWAT was treated with 1 μM oligomycin, 1 μM FCCP, 10 μM antimycin A, and 100 nM rotenone. The results were normalized to tissue weight [50].

Metabolic parameters measurements

Whole-body oxygen consumption and locomotor activity were determined by comprehensive lab animal monitoring system (Columbus Instruments, USA). For CL316,243 treatment, mice were i.p. injected with 1mg/kg CL316,243 (HY-116771A, MCE, China). Indirect calorimetry data were analyzed using ANCOVA/Generalized Linear Model with body mass as a covariate in CaIR (version 1.3, https://calrapp.org/). The body compositions of mice were measured by Bruker minispec NMR.

Rectal temperature was measured by digital thermometer (Physitemp Instruments, USA). For cold exposure, mice were singly housed in a cage without food, water or bedding.

Blood glucose levels were measured with a Glucometer (Abbott, USA). Serum insulin levels were measured by a commercial ELISA kit (ALPCO, USA). For glucose tolerance test (GTT), mice were i.p. injected with 2g/kg glucose after overnight fasting. For insulin tolerance test [55], mice were i.p. injected with 0.75 units/kg insulin after 4 h of fasting.

Histological analysis

sWAT and BAT were fixed in 4 % paraformaldehyde (PFA) and then subjected to hematoxylin and eosin (H&E) staining or immunostaining with anti-UCP1 antibody (1:4000, Abcam, ab209483/ab10983) by ServiceBio Co., Ltd. (China). Images were obtained using SLIDEVIEW VS200 SILA (Olympus, Japan).

AUH enzymatic activity assay

The AUH enzymatic activity was measured in the reverse direction [34,56]. The cells were harvested and washed with phosphate-buffered saline (PBS). The cells were then resuspended in PBS and homogenized using grinding beads. After centrifugation, 30 µL supernatant was mixed with 30 µL assay buffer (200 mM Tris-HCl pH 8.0, 20 mM EDTA, 2 mg/mL BSA, 0.2 mM HMG-CoA). After incubation at 37 °C for 1h, the reaction was terminated by addition of 6 µL 2 M HCl. The samples were homogenized, placed on ice for 5 min, and neutralized with 6 µL 2 M KOH. After centrifugation, 50 µL supernatant was used to evaluate the 3-MG-CoA levels using an ELISA kit (TSZ Biosciences, USA). The results were normalized to the cellular protein concentration.

Quantification of Leu metabolites

LC-MS/MS-based quantification of Leu metabolites in adipose tissue was conducted by Shanghai ProfLeader Biotech Co., Ltd. (China). BAT (40 ± 2 mg) or WAT (200 ± 4 mg) spiked with 40 µL acetyl-1,2-$^{13}C_2$-CoA as internal standard, was homogenized in 1 mL of extraction buffer (acetonitrile/isoproptanol/water/acetic acid, 9:3:4:4) by TissueLyser. The supernatant was collected, and the extraction step was repeated. The supernatant from twice extractions was combined and purified [57]. The eluates were evaporated to dryness and reconstituted in 50 µL of 20 % aqueous acetonitrile prior to UHPLC-MS/MS analysis. All acyl coenzyme A standards were prepared separately and mixed to a 1 µM

of mixed standard solution. The mixed standard solution was serially diluted, and finally mixed isometrically with stable isotope labeled internal standards (2 μg/mL) to obtain the standard curve samples with the concentration range of 1-500 nM. The UHPLC-MS/MS analysis was performed on an Agilent 1290 Infinity II UHPLC system coupled to a 6470A Triple Quadrupole mass spectrometry. Samples were injected onto a Waters BEH C18 column (100 mm × 2.1 mm, 1.7 μm) at a flow rate of 0.35 mL/min. The mobile phase consisted of (A) water in 5 mM ammonium acetate and (B) acetonitrile. The chromatographic separation was conducted by a gradient elution program as follows: 0-1 min, 1 % B; 1.1 min, 5 % B; 4 min, 10 % B; 12-13 min, 100 % B; 13.1-15 min, 1 % B. The eluted samples were ionized in an electro spray ionization source in positive mode. The temperatures of source drying gas and sheath gas were 300 °C and 350 °C, respectively. The flow rate of source drying gas and sheath gas were 5 and 11 L/min, respectively. The pressure of nebulizer was 40 psi, and capillary voltage was 4000 V. The dynamic multiple reaction monitoring (dMRM) was used to acquire data in optimized MRM transition (precursor -> product), fragmentor and collision energy (CE). MassHunter software (version B.08.00, Agilent) was used to control instruments and acquire data. The raw data were processed by MassHunter Workstation Software (version B.08.00, Agilent) using the default parameters and assisting manual inspection to ensure the qualitative and quantitative accuracies of each compound. The peak areas of each compound in all samples were integrated. Calibration curves of eleven-point were constructed by plotting the peak area ratio of each compound to internal standard against concentration of each compound. The concentrations of coenzyme A in prepared sample were quantified automatically. HMG-CoA levels in cells were measured using an ELISA kit (TSZ Biosciences, USA).

Protein purification

Glutathione Sepharose 4B (Cytiva, Sweden) was used to purify the GST-tagged recombinant WT and mutant mouse AUH proteins. *E. coli*. BL21 (DE3) cells carrying pGEX-4T-1-AUH were grown at

37 ℃ in LB medium with 100 mg/L ampicillin until OD_{600}=0.6-0.8. Cultures were induced with 0.2 mM isopropyl β-D-1- thiogalactopyranoside (IPTG) and grown at 16 °C for 16h. Cells were harvested by centrifugation at 8000×g for 10 min at 4 °C, then pellets were resuspended in 30 mL lysis buffer (50 mM Tris-HCl pH 8.0, 300 mM NaCl) supplemented with 100 μL 50 mg/mL lysozyme (Beyotime, China), 150U DNase I (Takara, Japan), 75 μL 4 M $MgCl_2$, and protease inhibitor cocktail (Roche, Switzerland). The mixture was sonicated using an ultrasonic processor and incubated overnight with Glutathione Sepharose 4B. After washing with lysis buffer and 50 mM Tris-HCl (pH 8.0), the protein was eluted with elution buffer (50 mM Tris-HCl pH 8.0, 10 mM GSH) and concentrated in Amicon@ Ultra Centrifugal filters (Merck, USA) of 30 kDa. Purified proteins were stored at -80 °C. Purified human PPARγ and PRDM16 proteins were purchased from Sino Biologcial Inc. (China) and OriGene (China), respectively.

RNA extraction and quantitative real-time PCR (RT-qPCR)

Total RNA was extracted from cells or mouse tissues using TRIzol regent (Invitrogen, USA). PrimeScript™ RT reagent Kit (Takara Bio, Japan) was used to perform reverse transcription. SYBR Green I Master Mix reagent and ABI QuantStudio™ 5 Real-Time PCR System (Applied Biosystems, USA) were used for RT-qPCR. The sequences of primers are listed in Supplementary Table 1.

Western blotting

Cells or mouse tissues were homogenized in RIPA buffer (150 mM NaCl, 25 mM Tris-HCl pH 8.0, 1 % NP-40, 0.1 % SDS). Samples were centrifuged at 12,000×g for 20 min at 4 ℃, and the supernatant was collected. The protein concentration was determined using a BCA Protein Assay Kit (Thermo Fisher Scientific, USA). Protein lysates were boiled with 5×SDS loading buffer (312.5mM Tris-HCl pH 6.8, 10 % SDS, 50 % glycerol, 20 % β-mercaptoethanol and 0.01 % bromophenol blue) at 100 ℃ for 10 min. The protein (20-30 μg) was separated by 10 or 12 % SDS-PAGE gel and transferred to a polyvinylidene

difluoride (PVDF) membrane (Merck, USA). Primary antibodies were diluted in TBS-T (Tris-HCl pH 7.6, 0.8 % NaCl, 0.05 % Tween-20) with 5 % BSA (Beyotime, China) and ProClin 300 (Merck, USA). Membranes were incubated with primary antibodies at 4 ℃ overnight. The anti-rabbit or anti-mouse secondary antibodies (Jackson Laboratory, USA) were diluted in TBS-T containing 5 % skimmed milk. Protein bands were visualized with ECL Plus reagents (Beyotime, China). The following antibodies were used for western blotting: anti-UCP1 (Abcam, ab209483), anti-AUH (Proteintech, 17079-1-AP), anti-PPARγ (Proteintech, 16643-1-AP), anti-PGC1-α (Merck, ST1202), anti-PRDM16 (R&D Systems, AF6295), anti-HMG-Lysine (Merck, ABS2108), anti-FLAG (Proteintech, 66008-4-Ig), anti-β-Actin (Proteintech, 66009-1-Ig).

Immunoprecipitation assay

Mice adipose tissue or primary adipocytes were lysed in ice-cold lysis buffer (50 mM Tris-HCl pH 7.5, 250 mM NaCl, 1% Triton X-100, 2 mM EGTA, 2 mM EDTA, and protease inhibitor cocktail) according to published protocols [21]. Briefly, the lysate was incubated on ice for 30 min, and then centrifuged at 12,000×g for 30 min at 4 °C. The supernatant was incubated with PPARγ primary antibodies (Proteintech, 16643-1-AP) and Protein A/G Agarose beads (Santa Cruz, USA) overnight at 4 °C. The beads were then washed 5 times with lysis buffer and the proteins were eluted by incubating the beads with 80 μL elution buffer (0.2 M Tris pH 6.8, 50 % glycerol, 10 % SDS, 0.01 % bromophenol blue). The eluted proteins were run on 4-20 % Bis-Tris polyacrylamide gels (Yeasen, China). The proteins were transferred onto PVDF membranes and blocked for 1.3 h in 1 % w/v fish gelatin in PBS. Membranes were incubated with primary antibodies in a 1:1 mixture of 1 % w/v fish gelatin/PBS and PBS + 0.05 % Tween 20 (PBST) overnight at 4 ℃. Secondary antibodies were diluted in the buffer same as primary antibodies.

In vitro incubation of proteins with HMG-CoA

HMG-CoA was purchased from Sigma and stored at -80 ℃ until use. Purified PPARγ or PRDM16 proteins were incubated with 0.5 or 1 mM HMG-CoA (final concentration). The assay mixture contained 50 mM HEPES and 150 mM NaCl, and was adjusted to pH 8.0. The reactions were incubated in a PCR amplifier at 37 ℃ for different periods of time as indicated [20]. After the incubation, loading buffer (0.2 M Tris pH 6.8, 50 % glycerol, 10 % SDS, 0.01 % bromophenol blue) was added. The samples were run on 4-20 % Bis-Tris polyacrylamide gels (Yeasen, China), followed by western blotting as performed in an immunoprecipitation assay.

Identification of HMGylation sites via mass spectrometry

4D-DIA proteomics was carried out by PTM Bio (Hangzhou, China). Purified human PPARγ proteins were incubate with HMG-CoA at 37 ℃ for 6 h in thermal cycler (n=1). For digestion, trypsin was added at 1:50 trypsin-to-protein mass ratio for the first digestion overnight. The protein solution was reduced with 5 mM dithiothreitol for 60 min at 37 °C and alkylated with 11 mM iodoacetamide for 45 min at room temperature in darkness. Finally, trypsin was added at 1:100 trypsin-to-protein mass ratio for a second 4 h-digestion. Peptides were first desalted using Strata X solid-phase extraction columns. The resulting tryptic peptides were reconstituted in solvent A and subsequently loaded onto a self-packed reversed-phase analytical column (25 cm in length, 100 μm inner diameter). Chromatographic separation was carried out on an EASY-nLC 1200 UPLC system (Thermo Fisher Scientific, USA) using a binary solvent system consisting of solvent A (0.1 % formic acid in water with 2 % acetonitrile) and solvent B (0.1 % formic acid in 90 % acetonitrile). Peptides were eluted at a constant flow rate of 700 nL/min with a segmented gradient as follows: 6 % to 22 % solvent B over 0–22.5 min, 22 % to 34 % over 22.5–26.5 min, 34 % to 80 % over 26.5–28.5 min, followed by a hold at 80 % until 30 min. Eluted peptides were analyzed using an Orbitrap Exploris 480 mass spectrometer equipped with a nano-electrospray ionization source. The spray voltage was set to 2.3 kV, and FAIMS compensation voltage was maintained at −45 V.

Both precursor and fragment ions were detected in the Orbitrap analyzer. Full MS scans were acquired over an m/z range of 350–1400 at a resolution of 60,000. MS/MS spectra were collected at a resolution of 15,000 with a fixed first mass of 120 m/z. Peptide fragmentation was performed using higher-energy collisional dissociation (HCD) with a normalized collision energy of 27 %. The automatic gain control (AGC) target was set to 1×10^6, and the maximum injection time was 22 ms. The DIA data were processed using Spectronaut (v.18) software. Tandem mass spectra were searched against the Homo_sapiens_9606_SP_20231220.fasta (20429 entries) concatenated with reverse decoy database. Trypsin/P was specified as cleavage enzyme allowing up to 4 missing cleavages. Carbamidomethyl on Cys was specified as fixed modification. Acetylation on protein N-terminal, oxidation on Met and HMG on Lys were specified as variable modifications. False discovery rate (FDR) of protein was adjusted to < 100 %, FDR of peptide and PSM was adjusted to < 5 %.

***In vitro* HMGylation assay**

Plasmids expressing FLAG-PPARγ (human) and its mutants were transfected into HEK293 cells (SCSP-5209, purchased from Cell Bank of Chinese Academy of Sciences) for 48 h, then proteins were extracted using lysis buffer (50 mM Tris-HCl pH 7.5, 250 mM NaCl, 1 % Triton X-100, 2 mM EGTA, 2 mM EDTA, and protease inhibitor cocktail). The PPARγ protein was pulled down and purified with anti-FLAG magnetic agarose beads (MBL, Japan). The beads were incubated with 1 mM HMG-CoA (final concentration) in a thermal cycler at 37 ℃ for 6 h and eluted by boiling in elution buffer (0.2 M Tris pH 6.8, 50 % glycerol, 10 % SDS, 0.01 % bromophenol blue) for 10 min. The supernatant was run on 4-20 % Bis-Tris polyacrylamide gels, followed by western blotting as performed in an immunoprecipitation assay.

RNA immunoprecipitation assay

RNA immunoprecipitation (RIP) assay was performed using the PureBinding@ RNA

Immunoprecipitation Kit (Geneseed Biotech, China). Briefly, BAT was lysed in lysis buffer. The extract was then immunoprecipitated with antibodies and protein A/G beads. RNA was isolated by columns in the kit and subjected to sequencing or RT-qPCR. For high-throughput sequencing (RIP-Seq), BAT from WT mice injected with AAV-AUH and anti-FLAG (Proteintech, 66008-4-Ig) or anti-mouse IgG (Proteintech, B900620) antibodies were used. RIP-Seq analysis was carried out by RiboBio Co., Ltd (China). For RIP-qPCR, BAT from WT mice and anti-AUH (Proteintech, 14861-1-AP) or anti-rabbit IgG (CST, 2729) antibodies were used.

PPARγ DNA-binding activity assay

Nuclear extracts of adipocytes were prepared using a Nuclear Protein Extraction Kit (Beyotime, China). PPARγ DNA-binding activity was measured using a PPARγ Transcription Factor Assay Kit (Abcam, USA) according to the manufacturer instructions.

Luciferase assay

HEK293 cells were co-transfected with indicated plasmids using Lipofectamine 2000 (Invitrogen, USA). The firefly and Renilla luciferase activities were measured by Dual-Luciferase Reporter Assay System (Promega, USA) and Lumate LB9508 (Berthod, Germany).

Chromatin immunoprecipitation Assay

Chromatin immunoprecipitation (ChIP) assay was performed using a BeyoChIP^{TM} Enzymatic ChIP Assay Kit (Beyotime, China). In brief, differentiated primary brown adipocytes in 10 cm dishes were fixed with 1 % formaldehyde for 10 min at 37 ℃, followed by adding glycine to quench unreacted formaldehyde. Micrococcal nucleases in the kit and an ultrasonic processor were used for chromatin fragmentation. Immunoprecipitation was performed with protein A/G magnetic beads from the kit and

anti-PPARγ (Proteintech, 16643-1-AP) or anti-IgG (CST, 2729) antibody at 4 ℃ overnight, followed by washing and elution. The ChIPed DNA was purified using tris-phenol/chloroform and quantified by RT-qPCR.

RNA pull-down assay

RNA pull-down assay was performed using the Pierce™ Magnetic RNA-Protein Pull-Down Kit (Thermo Fisher Scientific, USA). *Ucp1-3′ UTR* RNA was synthesized in vitro by T7 RNA polymerase-mediated transcription. Purified mouse AUH and the mutant proteins were prepared as described above. Briefly, T4 RNA ligase was used to attach a single desthiobiotinylated cytidine bisphosphate to the 3′ end of the *Ucp1-3'UTR* RNA and the negative control poly(A)$_{25}$ RNA strand. The labeled RNA was bound to streptavidin magnetic beads and incubated with purified AUH proteins. The samples were washed and eluted with biotin elution buffer. The supernatant was boiled in reducing sample buffer for 10 min at 100 ℃ for western blot analysis.

RNA decay analysis

Primary brown adipocytes were transfected with si-*Auh* or si-NC for 72 h, and with plasmids expressing WT AUH, mutant AUH, or empty vectors for 48 h. Then, the cells were treated with 10 μg/mL actinomycin D (MCE, China), and RNA was harvested at different time points as indicated. Total RNA was extracted by TRIzol regent, and RT-qPCR was conducted to calculate the remaining percentage of mRNA at each point. Data were fit into a first-phase decay model to derive mRNA half-life,

$Y_t = (Y_0 - \text{Plateau}) \times \exp(-K_{decay} \times t) + \text{Plateau}$

with Y_t: the remaining percentage at a given time, Y_0: the initial amount of RNA, t: time after transcription inhibition, and K_{decay}: the rate constant [58].

Statistics and Reproducibility ~~Quantification and statistical analysis~~

Data were represented as "mean ± S.E.M." and analyzed using GraphPad Prism 8.0 (GraphPad Software, Inc., USA). Mean ± SEM are representative of at least two (in vivo) or three (in vitro) independent experiments. Two-tailed Student's t-test was used to compare the mean of two groups. For multiple comparisons, ordinary one-way ANOVA, two-way ANOVA or two-way RM ANOVA with Geisser-Greenhouse's correction was used, followed by Dunnett's or Tukey's multiple comparisons test. The statistical details were indicated in the figure legend. Results were considered statistically significant when the *P* value was less than 0.05.

Data Availability

Data supporting the findings of this study are available within this paper and its Supplementary Files. The RIP-Seq data generated in this study have been deposited into the Sequence Read Archive (SRA) in National Center for Biotechnology Information (NCBI) under the accession codes PRJNA1301336. The mass spectrometry proteomics data have been deposited to the ProteomeXchange Consortium via the iProX partner repository with the dataset identifier PXD075390. The RNA-Seq data used in this study are available in the NCBI Gene Expression Omnibus (GEO) database under accession codes GSE152991 and GSE166047. Source data are provided with this paper.

References

1 Chen, K. Y. *et al.* Opportunities and challenges in the therapeutic activation of human energy expenditure and thermogenesis to manage obesity. *The Journal of biological chemistry* **295**, 1926-1942, doi:10.1074/jbc.REV119.007363 (2020).

2 Newgard, C. B. *et al.* A branched-chain amino acid-related metabolic signature that differentiates obese and lean humans and contributes to insulin resistance. *Cell metabolism* **9**, 311-326, doi:10.1016/j.cmet.2009.02.002 (2009).

3 Felig, P., Marliss, E. & Cahill, G. F., Jr. Plasma amino acid levels and insulin secretion in obesity. *N Engl J Med* **281**, 811-816, doi:10.1056/nejm196910092811503 (1969).

4 Xiao, F. & Guo, F. Impacts of essential amino acids on energy balance. *Molecular metabolism* **57**, 101393, doi:10.1016/j.molmet.2021.101393 (2022).

5 Yoneshiro, T. *et al.* BCAA catabolism in brown fat controls energy homeostasis through SLC25A44. *Nature* **572**, 614-

619, doi:10.1038/s41586-019-1503-x (2019).

6 Cannavino, J. *et al.* Regulation of cold-induced thermogenesis by the RNA binding protein FAM195A. *Proceedings of the National Academy of Sciences of the United States of America* **118**, doi:10.1073/pnas.2104650118 (2021).

7 Ananieva, E. A., Powell, J. D. & Hutson, S. M. Leucine Metabolism in T Cell Activation: mTOR Signaling and Beyond. *Adv Nutr* **7**, 798s-805s, doi:10.3945/an.115.011221 (2016).

8 Jiang, H., Guo, F. & Xiao, F. Role of Branched-Chain Amino Acid Catabolism in the Regulation of Adipocyte Metabolism. *Endocrinology* **166**, doi:10.1210/endocr/bqaf089 (2025).

9 Nakagawa, J. *et al.* AUH, a gene encoding an AU-specific RNA binding protein with intrinsic enoyl-CoA hydratase activity. *Proceedings of the National Academy of Sciences of the United States of America* **92**, 2051-2055, doi:10.1073/pnas.92.6.2051 (1995).

10 Mack, M. *et al.* Biochemical characterization of human 3-methylglutaconyl-CoA hydratase and its role in leucine metabolism. *FEBS J* **273**, 2012-2022, doi:10.1111/j.1742-4658.2006.05218.x (2006).

11 Ma, Q. X. *et al.* BCAA-BCKA axis regulates WAT browning through acetylation of PRDM16. *Nature metabolism* **4**, 106-122, doi:10.1038/s42255-021-00520-6 (2022).

12 Gross, B., Pawlak, M., Lefebvre, P. & Staels, B. PPARs in obesity-induced T2DM, dyslipidaemia and NAFLD. *Nat Rev Endocrinol* **13**, 36-49 (2017).

13 Dubois, V., Eeckhoute, J., Lefebvre, P. & Staels, B. Distinct but complementary contributions of PPAR isotypes to energy homeostasis. *J Clin Invest* **127**, 1202-1214 (2017).

14 Xiong, W. *et al.* Brown Adipocyte-Specific PPARγ (Peroxisome Proliferator-Activated Receptor γ) Deletion Impairs Perivascular Adipose Tissue Development and Enhances Atherosclerosis in Mice. *Arterioscler Thromb Vasc Biol* **38**, 1738-1747, doi:10.1161/atvbaha.118.311367 (2018).

15 Brunmeir, R. & Xu, F. Functional Regulation of PPARs through Post-Translational Modifications. *Int J Mol Sci* **19**, doi:10.3390/ijms19061738 (2018).

16 Dai, N. *et al.* IGF2BP2/IMP2-Deficient mice resist obesity through enhanced translation of Ucp1 mRNA and Other mRNAs encoding mitochondrial proteins. *Cell metabolism* **21**, 609-621, doi:10.1016/j.cmet.2015.03.006 (2015).

17 Takahashi, A. *et al.* Post-transcriptional Stabilization of Ucp1 mRNA Protects Mice from Diet-Induced Obesity. *Cell Rep* **13**, 2756-2767, doi:10.1016/j.celrep.2015.11.056 (2015).

18 Sustarsic, E. G. *et al.* Cardiolipin Synthesis in Brown and Beige Fat Mitochondria Is Essential for Systemic Energy Homeostasis. *Cell metabolism* **28**, 159-174.e111, doi:10.1016/j.cmet.2018.05.003 (2018).

19 Chen, Y. *et al.* Adipocyte IRE1α promotes PGC1α mRNA decay and restrains adaptive thermogenesis. *Nature metabolism* **4**, 1166-1184, doi:10.1038/s42255-022-00631-8 (2022).

20 Wagner, G. R. *et al.* A Class of Reactive Acyl-CoA Species Reveals the Non-enzymatic Origins of Protein Acylation. *Cell metabolism* **25**, 823-837 e828, doi:10.1016/j.cmet.2017.03.006 (2017).

21 Trub, A. G. *et al.* Statin therapy inhibits fatty acid synthase via dynamic protein modifications. *Nat Commun* **13**, 2542, doi:10.1038/s41467-022-30060-w (2022).

22 Richman, T. R. *et al.* A bifunctional protein regulates mitochondrial protein synthesis. *Nucleic Acids Res* **42**, 5483-5494, doi:10.1093/nar/gku179 (2014).

23 Kurimoto, K., Fukai, S., Nureki, O., Muto, Y. & Yokoyama, S. Crystal structure of human AUH protein, a single-stranded RNA binding homolog of enoyl-CoA hydratase. *Structure* **9**, 1253-1263, doi:10.1016/s0969-2126(01)00686-4 (2001).

24 Shaw, G. & Kamen, R. A conserved AU sequence from the 3' untranslated region of GM-CSF mRNA mediates selective mRNA degradation. *Cell* **46**, 659-667, doi:10.1016/0092-8674(86)90341-7 (1986).

25 Cifarelli, V. *et al.* Decreased adipose tissue oxygenation associates with insulin resistance in individuals with obesity. *J Clin Invest* **130**, 6688-6699, doi:10.1172/jci141828 (2020).

26 Messa, L. *et al.* RNA-seq dataset of subcutaneous adipose tissue: Transcriptional differences between obesity and healthy women. *Data Brief* **39**, 107647, doi:10.1016/j.dib.2021.107647 (2021).

27 Liu, Y., Qian, S. W., Tang, Y. & Tang, Q. Q. The secretory function of adipose tissues in metabolic regulation. *Life metabolism* **3**, loae003, doi:10.1093/lifemeta/loae003 (2024).

28 Cao, Z. *et al.* Methylcrotonoyl-CoA carboxylase 1 potentiates RLR-induced NF-κB signaling by targeting MAVS complex. *Sci Rep* **6**, 33557, doi:10.1038/srep33557 (2016).

29 Wirth, M. *et al.* Mitochondrial SIRT4-type proteins in Caenorhabditis elegans and mammals interact with pyruvate carboxylase and other acetylated biotin-dependent carboxylases. *Mitochondrion* **13**, 705-720, doi:10.1016/j.mito.2013.02.002 (2013).

30 Anderson, K. A. *et al.* SIRT4 Is a Lysine Deacylase that Controls Leucine Metabolism and Insulin Secretion. *Cell metabolism* **25**, 838-855.e815, doi:10.1016/j.cmet.2017.03.003 (2017).

31 Chen, Y. Y. *et al.* MCCC2 promotes HCC development by supporting leucine oncogenic function. *Cancer Cell Int* **21**, 22, doi:10.1186/s12935-020-01722-w (2021).

32 Brennan, L. E., Nakagawa, J., Egger, D., Bienz, K. & Moroni, C. Characterisation and mitochondrial localisation of AUH, an AU-specific RNA-binding enoyl-CoA hydratase. *Gene* **228**, 85-91, doi:10.1016/s0378-1119(99)00003-7 (1999).

33 Ly, T. B. *et al.* Mutations in the AUH gene cause 3-methylglutaconic aciduria type I. *Hum Mutat* **21**, 401-407, doi:10.1002/humu.10202 (2003).

34 L, I. J. *et al.* 3-Methylglutaconic aciduria type I is caused by mutations in AUH. *Am J Hum Genet* **71**, 1463-1466, doi:10.1086/344712 (2002).

35 Chen, G., Huang, L. D., Zeng, W. Z. & H, K. M. Mood stabilizers regulate cytoprotective and mRNA-binding proteins in the brain: long-term effects on cell survival and transcript stability. *Int J Neuropsychopharmacol* **4**, 47-64, doi:10.1017/s146114570100222x (2001).

36 Okamatsu-Ogura, Y., Kitao, N., Kimura, K. & Saito, M. Brown fat UCP1 is not involved in the febrile and thermogenic responses to IL-1beta in mice. *American journal of physiology. Endocrinology and metabolism* **292**, E1135-1139, doi:10.1152/ajpendo.00425.2006 (2007).

37 Balaz, M. *et al.* Inhibition of Mevalonate Pathway Prevents Adipocyte Browning in Mice and Men by Affecting Protein Prenylation. *Cell metabolism* **29**, 901-916.e908, doi:10.1016/j.cmet.2018.11.017 (2019).

38 Kwon, J. *et al.* Mevalonate biosynthesis pathway regulates the development and survival of brown adipocytes. *iScience* **26**, 106161, doi:10.1016/j.isci.2023.106161 (2023).

39 Nguyen, H. P. *et al.* Aifm2, a NADH Oxidase, Supports Robust Glycolysis and Is Required for Cold- and Diet-Induced Thermogenesis. *Molecular cell* **77**, 600-617.e604, doi:10.1016/j.molcel.2019.12.002 (2020).

40 Cypess, A. M. *et al.* Identification and importance of brown adipose tissue in adult humans. *N Engl J Med* **360**, 1509-1517, doi:10.1056/NEJMoa0810780 (2009).

41 Chouchani, E. T., Kazak, L. & Spiegelman, B. M. New Advances in Adaptive Thermogenesis: UCP1 and Beyond. *Cell metabolism* **29**, 27-37, doi:10.1016/j.cmet.2018.11.002 (2019).

42 Martínez-Reyes, I. & Chandel, N. S. Mitochondrial TCA cycle metabolites control physiology and disease. *Nat Commun* **11**, 102, doi:10.1038/s41467-019-13668-3 (2020).

43 Aaron, N. *et al.* Acetylation of PPARγ in macrophages promotes visceral fat degeneration in obesity. *Life metabolism* **1**, 258-269, doi:10.1093/lifemeta/loac032 (2022).

44 Jiang, X., Ye, X., Guo, W., Lu, H. & Gao, Z. Inhibition of HDAC3 promotes ligand-independent PPARγ activation by protein acetylation. *Journal of molecular endocrinology* **53**, 191-200, doi:10.1530/jme-14-0066 (2014).

45 Villarroya, F., Peyrou, M. & Giralt, M. Transcriptional regulation of the uncoupling protein-1 gene. *Biochimie* **134**, 86-92, doi:10.1016/j.biochi.2016.09.017 (2017).

46 Chen, H. F., Hsu, C. M. & Huang, Y. S. CPEB2-dependent translation of long 3'-UTR Ucp1 mRNA promotes thermogenesis in brown adipose tissue. *Embo j* **37**, doi:10.15252/embj.201899071 (2018).

47 Lu, H. *et al.* QKI regulates adipose tissue metabolism by acting as a brake on thermogenesis and promoting obesity. *EMBO Rep* **21**, e47929, doi:10.15252/embr.201947929 (2020).

48 Maniyadath, B., Zhang, Q., Gupta, R. K. & Mandrup, S. Adipose tissue at single-cell resolution. *Cell metabolism* **35**, 386-413, doi:10.1016/j.cmet.2023.02.002 (2023).

49 Bartelt, A. & Heeren, J. Adipose tissue browning and metabolic health. *Nat Rev Endocrinol* **10**, 24-36, doi:10.1038/nrendo.2013.204 (2014).

50 Xiao, F. *et al.* Reduced hepatic bradykinin degradation accounts for cold-induced BAT thermogenesis and WAT browning in male mice. *Nat Commun* **14**, 2523, doi:10.1038/s41467-023-38141-0 (2023).

51 Deng, J. *et al.* Autophagy inhibition prevents glucocorticoid-increased adiposity via suppressing BAT whitening. *Autophagy* **16**, 451-465, doi:10.1080/15548627.2019.1628537 (2020).

52 Li, Y., Fromme, T., Schweizer, S., Schöttl, T. & Klingenspor, M. Taking control over intracellular fatty acid levels is essential for the analysis of thermogenic function in cultured primary brown and brite/beige adipocytes. *EMBO reports* **15**, 1069-1076, doi:10.15252/embr.201438775 (2014).

53 Li, Y. & Fromme, T. Uncoupling Protein 1 Does Not Produce Heat without Activation. *International journal of molecular sciences* **23**, doi:10.3390/ijms23052406 (2022).

54 Fromme, T. *et al.* Degradation of brown adipocyte purine nucleotides regulates uncoupling protein 1 activity. *Molecular metabolism* **8**, 77-85, doi:10.1016/j.molmet.2017.12.010 (2018).

55 Whittle, A. J. *et al.* BMP8B increases brown adipose tissue thermogenesis through both central and peripheral actions. *Cell* **149**, 871-885, doi:10.1016/j.cell.2012.02.066 (2012).

56 Loupatty, F. J., Ruiter, J. P., L, I. J., Duran, M. & Wanders, R. J. Direct nonisotopic assay of 3-methylglutaconyl-CoA hydratase in cultured human skin fibroblasts to specifically identify patients with 3-methylglutaconic aciduria type I. *Clin Chem* **50**, 1447-1450, doi:10.1373/clinchem.2004.033142 (2004).

57 Minkler, P. E., Kerner, J., Ingalls, S. T. & Hoppel, C. L. Novel isolation procedure for short-, medium-, and long-chain acyl-coenzyme A esters from tissue. *Analytical biochemistry* **376**, 275-276, doi:10.1016/j.ab.2008.02.022 (2008).

58 Siang, D. T. C. *et al.* The RNA-binding protein HuR is a negative regulator in adipogenesis. *Nat Commun* **11**, 213, doi:10.1038/s41467-019-14001-8 (2020).

Acknowledgements

This work was supported by grants from the National Natural Science Foundation of China (82430030, 82495182, 92357304 and 91957207 to F.G., 82270905 to F.X., 82401017 to H.J., 82370811 to F.Y., 82300939 to X.J., 82300940 to Y.N.), the National Key R&D Program of China

(2018YFA0800600 to F.G.), Shanghai leading talent program to F.G, and Postdoctoral Fellowship Program of China Postdoctoral Science Foundation (GZC20230478 to H.J.). F.X. was sponsored by Youth Innovation Promotion Association of CAS, Shanghai Rising Star Program and Sanofi-Aventis SIBS scholarship. H.J. was sponsored by Fudan University Super Postdoctoral Fellowship.

Author contributions

H.J. and F.X. designed and carried out overall experiments, analyzed data, wrote, reviewed and edited the manuscript. S.N., S.C., X.J., P.L., F.Y. and K.T. assisted with mouse experiments and cultured cell studies. Z.L. developed the LC-MS/MS platform to measure the HMG-CoA levels. X.L., H.Z., W.S. and Y.S. provided research materials and contributed to discussion. F.G. directed the research, contributed to discussion, wrote, reviewed and edited the manuscript.

Competing interests: The authors declare no competing interests.

Figure Legends

Figure 1. AUH regulates UCP1 expression in primary brown adipocytes

a-c mRNA levels of *Auh* and *Ucp1* (**a**), protein levels of AUH and UCP1 (**b**), and oxygen consumption rate (OCR, **c**) were examined in primary brown adipocytes transfected with small interfering RNA (siRNA) targeting *Auh* (si-*Auh*-1 and -2) or control (si-NC) for 72 h. **d-f** mRNA levels of *Auh* and *Ucp1* (**d**), protein levels of UCP1 (**e**), and OCR (**f**) were examined in primary brown adipocytes infected with adenoviruses expressing AUH (+Ad-AUH) or control GFP (–Ad-AUH) for 48 h. For **a**, n = 6 in each group. For **b** and

e, n = 4 in each group. For **c** and **f**, n = 5 in each group. For **d**, n = 7 in each group. Data are represented as mean ± SEM; two-tailed unpaired Student's t-test (**a-f**). Source data are provided as a Source Data file.

Figure 2. AUH knockdown reduces BAT thermogenesis

Analyses of metabolic parameters in male WT mice with BAT injection of AAV-shAUH (+AAV-shAUH) or AAV-scramble (–AAV-shAUH), including mRNA levels of *Auh* and *Ucp1* in BAT (**a**), protein levels of AUH and UCP1 in BAT (**b**), oxygen consumption rate (OCR) in BAT (**c**), whole-body oxygen consumption without (**d**) or with 1mg/kg CL316,243 injection (**e**), rectal temperature at 24℃ (**f**) or following cold exposure at 4 ℃ (**g**). For **e** (right panel), the changes were calculated from the middle panel as the difference between the value after CL316,243 injection and the baseline value. For **a**-**d**, **g**, n = 6 mice per group. For **e**, n = 5 mice per group. For **f**, n = 8 mice per group. Data are represented as mean ± SEM; two-tailed unpaired Student's t-test (**a-c**, **e right**, **f**), two-way RM ANOVA with Geisser-Green house's correction followed by post hoc unpaired t-test (**g**); indirect calorimetry data were analyzed using two-sided ANCOVA/ Generalized Linear Model with body mass as a covariate in CaIR (version 1.3, https:// calrapp.org/, **d**, **e middle**). Source data are provided as a Source Data file.

Figure 3. AUH deficiency inhibits BAT thermogenesis

Analyses of metabolic parameters in male $AUH^{flox/flox}$ and AUH-UKO mice, including mRNA levels of *Ucp1* in BAT (**a**), protein levels of AUH and UCP1 in BAT (**b**), oxygen consumption rate (OCR) in BAT (**c**), whole-body oxygen consumption without (**d**) or with 1mg/kg CL316,243 injection (**e**), rectal temperature at 24 ℃ (**f**) or following cold exposure at 4 ℃ (**g**). For **e** (right panel), the changes were

calculated from the middle panel as the difference between the value after CL316,243 injection and the baseline value. For **a**, **b**-**c** and **g**, n = 5 mice per group. For **d** and **f**, n = 7 mice per group. For **e,** n = 5 ($AUH^{flox/flox}$) and 6 (AUH-UKO) mice per group. Data are represented as mean ± SEM; two-tailed unpaired Student's t-test (**a-c**, **e right**, **f**), two-way RM ANOVA with Geisser-Green house's correction followed by post hoc unpaired t-test (**g**); indirect calorimetry data were analyzed using two-sided ANCOVA/ Generalized Linear Model with body mass as a covariate in CaIR (version 1.3, https:// calrapp.org/, **d**, **e middle**). Source data are provided as a Source Data file.

Figure 4. AUH overexpression increases BAT thermogenesis

Analyses of metabolic parameters in male WT mice with BAT injection of AAV-AUH (+AAV-AUH) or AAV-GFP (–AAV-AUH), including mRNA levels of *Ucp1* in BAT (**a**), protein levels of AUH and UCP1 in BAT (**b**), oxygen consumption rate (OCR) in BAT (**c**), whole-body oxygen consumption (**d**), rectal temperature at 24 ℃ (**e**) or following cold exposure at 4 ℃ (**f**), and fat mass (**g**). For **a**, **b**, **d** and **f,** n = 6 mice per group. For **c**, n = 5 (–AAV-AUH) and 6 (+AAV-AUH) mice per group. For **e**, n = 7 mice per group. For **g**, n = 5 mice per group. Data are represented as mean ± SEM; two-tailed unpaired Student's t-test (**a-c**, **e**, **g**), two-way RM ANOVA with Geisser-Green house's correction followed by post hoc unpaired t-test (**f**); indirect calorimetry data were analyzed using two-sided ANCOVA/ Generalized Linear Model with body mass as a covariate in CaIR (version 1.3, https:// calrapp.org/, **d**). Source data are provided as a Source Data file.

Figure 5. HMG-CoA contributes to the effects of AUH on PPARγ activity and UCP1 expression

a Scheme of the Leu catabolic pathway (left), and HMG-CoA content in the BAT of male WT mice with BAT injection of AAV-shAUH (+AAV-shAUH) or AAV-scramble (–AAV-shAUH, right). The arrows indicate the increase or decrease in the content of the corresponding metabolites in BAT of AAV-shAUH mice. **b**, **c** mRNA (**b**) and protein (**c**) levels of AUH and UCP1 in primary brown adipocytes transfected with si-*Auh* or si-NC for 72 h, followed by incubation with or without HMG-CoA for 1 h. **d**, **e** Protein levels of PPARγ, PRDM16, PGC1α, and AUH in the BAT of male WT mice with BAT injection of AAV-shAUH (+AAV-shAUH) or AAV-scramble (–AAV-shAUH, **d**), and AAV-AUH (+AAV-AUH) or AAV-GFP (–AAV-AUH, **e**). **f-h** Primary brown adipocytes were transfected with si-*Auh* or si-NC for 72 h, followed by incubation with or without 0.5 mM HMG-CoA for 1 h. PPARγ transcriptional activity was measured using the pPPARγ-Fluc-hRluc luciferase reporter assay system (**f**). PPARγ DNA-binding activity was measured using a PPARγ Transcription Factor Assay Kit from Abcam (**g**). ChIP assay was performed to assess PPARγ binding to the *Ucp1* promoter (**h**). **i** mRNA (left) and protein levels of UCP1 in primary brown adipocytes transfected with si-*Auh* or si-NC for 72 h and plasmids expressing mouse PPARγ (+PPARγ) or empty vectors (–PPARγ) for 48 h. For **a**, n = 6 mice per group. For **b**, n = 6 (*Auh* mRNA) and 5 (*Ucp1* mRNA) in each group. For **c**, n = 4 in each group. For **d**-**g**, n = 6 in each group. For **h**, n = 3 in each group. For **i**, n = 4 (–si-*Auh*–PPARγ) and 6 (–si-*Auh*+PPARγ, +si-*Auh*–PPARγ, +si-*Auh*+PPARγ) in each group (left); n = 5 in each group. Data are represented as mean ± SEM; two-tailed unpaired Student's t-test (**a**, **d**, **e**), ordinary one-way ANOVA with Tukey's test (**f-h**), ordinary two-way ANOVA with Tukey's multiple comparisons test (**i**). Source data are provided as a Source Data file.

Figure 6. AUH regulates HMGylation of PPARγ via HMG-CoA

a Total protein HMGylation levels of BAT from male Auh$^{flox/flox}$ and AUH-UKO mice. **b**, **c** BAT lysates of male WT mice after BAT injection with AAV-AUH (+AAV-AUH) or AAV-GFP (–AAV-AUH, **b**), with AAV-shAUH (+AAV-shAUH) or AAV-scramble (–AAV-shAUH, **c**) were immunoprecipitated (IP) with anti-PPARγ antibody followed by immunoblotting with the indicated antibodies. **d** Cell lysates from primary brown adipocytes transfected with si-*Auh* or si-NC for 72 h were immunoprecipitated (IP) with anti-PPARγ antibody followed by immunoblotting with the indicated antibodies. **e** Primary brown adipocytes were transfected with si-*Auh* or si-NC for 72 h and incubated with or without 0.5 mM HMG-CoA for 1 h. This was followed by immunoprecipitation using anti-PPARγ antibody and immunoblotting with the indicated antibodies. **f** Purified human PPARγ proteins were incubated with 0, 0.5 or 1 mM HMG-CoA at 37 ℃ for 6 h followed by immunoblotting with the indicated antibodies. **g** Purified human PPARγ was incubated with or without 0.5 mM HMG-CoA at 37 ℃ for 30 min followed by the detection of DNA-binding activity using a PPARγ Transcription Factor Assay Kit from Abcam. **h** HEK293 cells were co-transfected with plasmids expressing human PPARγ (+PPARγ) or empty vectors (–PPARγ) and pPPARγ-Fluc-hRluc luciferase reporter for 48 h, followed by incubating with or without 0.1 mM HMG-CoA for 30 min. Luciferase activity was then measured. For **g**, n = 3 (–HMG-CoA) and 4 (+HMG-CoA) in each group. For **h**, n = 5 in each group. For **a**-**f**, representative immunoblots from three independent experiments are shown. Data are represented as mean ± SEM; two-tailed unpaired Student's t-test (**g**), ordinary one-way ANOVA with Tukey's test (**h**). Source data are provided as a Source Data file.

Figure 7. PPARγ is HMGylated at lysine 386

a Scheme of PPARγ HMGylated lysine sites from LC-MS/MS analysis. All the identified HMGylated

lysine sites are marked in red. **b** Mass spectrum revealing lysine 386 of PPARγ as a HMGylation site. **c** HEK 293 cells were transfected with either WT or K386R human FLAG-PPARγ-expressing plasmids for 48 h, followed by immunoprecipitation with anti-FLAG magnetic beads, *in vitro* HMGylation assay, and immunoblotting with the indicated antibodies. **d** Lysine 386 of PPARγ is conserved in the indicated species. **e** HEK293 cells were co-transfected with either WT or K386R human FLAG-PPARγ-expressing plasmids and pPPARγ-Fluc-hRluc luciferase reporter for 48 h, followed by incubating with or without 0.1 mM HMG-CoA for 30 min. Luciferase activity was then measured. **f** *Ucp1* mRNA levels in primary brown adipocytes transfected with plasmids expressing WT or K386R mouse PPARγ for 48 h, followed by incubation with 0.5 mM HMG-CoA for 1 h. For **e**, n = 6 in each group. For **f**, n = 4 in each group. For **c**, representative immunoblots from three independent experiments are shown. Data are represented as mean ± SEM; two-tailed unpaired Student's t-test (**e**, **f**). Source data are provided as a Source Data file.

Figure 8. AUH targets and stabilizes *Ucp1* mRNA

a KEGG pathway enrichment analysis of AUH-binding transcripts in BAT from RIP-seq experiment. The top 10 genes from thermogenesis-related pathway are listed. **b** Distribution of AUH-binding peaks within the *Ucp1* mRNA region. The 3′ UTR region is framed out. **c** RNA immunoprecipitation (RIP) assay detecting AUH binding on *Ucp1* mRNA 3′ UTR in BAT lysates from male WT mice. **d** RNA pull-down assay using purified AUH proteins and in vitro transcribed *Ucp1* 3′ UTR mRNA fragments. **e**-**h** Primary brown adipocytes were transfected with si-*Auh* or si-NC for 72 h (**e**), with plasmids expressing WT AUH or empty vectors for 48 h (**f**), with plasmids expressing AUH-K80N/K84E/K88Q or empty vectors for 48 h (**g**), and with plasmids expressing AUH-A215V or empty vectors for 48 h (**h**). The cells were then

treated with actinomycin D. Remaining *Ucp1* mRNA and 18s rRNA levels were determined at the indicated time points. **i** Primary brown adipocytes were transfected with si-*Auh* or si-NC for 24 h and then transfected with luciferase-*Ucp1* 3′ UTR reporter for 48 h (left). Primary brown adipocytes were co-transfected with plasmids expressing WT AUH or empty vectors and luciferase-*Ucp1* 3′ UTR reporter for 48 h. Luciferase activity was then measured. For a, KEGG pathway enrichment analysis was performed using the clusterProfiler package (or KOBAS 3.0). Statistical significance of enrichment was determined using a one-sided hypergeometric test. p-values were adjusted for multiple comparisons, and an adjusted $p < 0.05$ was considered statistically significant. For **c**, n = 4 in each group. For **e** and **f**, n = 5 in each group. For **g** and **h**, n = 4 in each group. For **i**, n = 6 (left) and 5 in each group. For **d**, representative immunoblots from three independent experiments are shown. Data are represented as mean ± SEM; two-tailed unpaired Student's t-test (**c**, **i**). Source data are provided as a Source Data file.

Figure 9. AUH promotes sWAT browning

a-**e**, **h**, **i** mRNA levels of *Ucp1* in sWAT (**a**), protein levels of AUH and UCP1 in sWAT (**b**, left), representative immunohistochemistry (IHC) staining of UCP1 in sWAT (**b**, right), oxygen consumption rate (OCR) in sWAT (**c**), representative H&E staining of sWAT (**d**), sWAT weight (**e**), HMG-CoA levels (**h**) and PPARγ HMGylation (**i**) in sWAT from male WT mice after sWAT injection with AAV-AUH (+AAV-AUH) or AAV-GFP (–AAV-AUH). Scar bars, 50 μm (**b**, **d**). **f**, **g** mRNA levels of *Auh* and *Ucp1* (**f**), and the OCR (**g**) of primary white adipocytes infected with Ad-AUH (+Ad-AUH) or Ad-GFP (–Ad-AUH) for 48 h. **j** Cell lysates from primary white adipocytes infected with Ad-AUH (+Ad-AUH) or Ad-GFP (–Ad-AUH) for 48 h were immunoprecipitated (IP) with anti-PPARγ antibody followed by

immunoblotting with the indicated antibodies. For **a**, n = 10 mice per group. For **b**, **g** and **h**, n = 6 in each group. For **c** and **f**, n = 5 in each group. For **e**, n = 8 mice per group. For **i**, **j**, representative immunoblots from three independent experiments are shown. Data are represented as mean ± SEM; two-tailed unpaired Student's t-test (**a-c**, **e**, **f**, **h**), two-way RM ANOVA with Geisser-Greenhouse's correction (**g**). Source data are provided as a Source Data file.

Figure 10. AUH overexpression in adipose tissue protects mice against high-fat diet (HFD)-induced obesity

a *AUH* expression in the WAT of metabolic-healthy lean, metabolic-healthy or metabolic-unhealthy humans with obesity (corresponding to the "Metabolic-healthy Obese" and "Metabolic-unhealthy Obese" group) from GSE152991 dataset (left). *AUH* expression in the WAT of individuals with normal weight or obesity (corresponding to the "obese" group) from the GSE166047 dataset. In the box plot, the box spans the interquartile range (IQR, from the 25th to the 75th percentile), with the internal line indicating the median. The whiskers extend to the minimum and maximum values. All individual data points are overlaid as dots to visualize the data distribution. **b**, **c** AUH protein levels (**b**) and HMG-CoA content (**c**) in the sWAT of male WT mice fed a high-fat diet (HFD) or a normal chow diet (NCD) for 4 months. **d-j** Body weight (**d**), fat mass (**e**), tissue weight (**f**), mRNA (left) and protein levels of UCP1 and AUH in BAT (**g**), *Ucp1* mRNA levels in sWAT (**h**, left), representative immunohistochemistry (IHC) staining of UCP1 in sWAT ((**h**, right), representative H&E staining of sWAT (**i**), insulin tolerance test (ITT, **j** left), and glucose tolerance test (GTT, **j** right) from male WT mice after sWAT and BAT injections of AAV-AUH (+AAV-AUH) or AAV-GFP (–AAV-AUH). These mice were fed a HFD for 10 weeks. Scar bars, 50 μm (**h**, **i**). **k** Working model Created in BioRender. Jiang, H. (2025) https://BioRender.com/j5o4hwh. For **a**, n = 11 (Metabolic-healthy Lean), 13 (Metabolic-healthy Obese) and 20 (Metabolic-unhealthy Obese) in each

group (left); n= 4 in each group (right). For **b** and **c**, n = 6 mice per group. For **d**, **e**, **h** and **j**, n = 10 mice per group. For **f**, n = 8 mice per group. For **g**, n = 8 (left) and 5 mice per group. Data are represented as mean ± SEM; two-tailed unpaired Student's t-test (**a** right, **b**, **c**, **f-h**), ordinary one-way ANOVA with Tukey's test (**a** left), or two-way RM ANOVA with Geisser-Green house's correction followed by post hoc unpaired t-test (**d, e**, **j**). Source data are provided as a Source Data file.

Editorial summary:
The authors show that leucine metabolic enzyme AUH promotes fat burn and protects against obesity. AUH drives thermogenesis via Ucp1 mRNA stabilization and PPARγ modification via metabolite HMG-CoA, linking amino acid metabolism to weight regulation.

Peer review information: *Nature Communications* thanks the anonymous, reviewer(s) for their contribution to the peer review of this work. A peer review file is available.

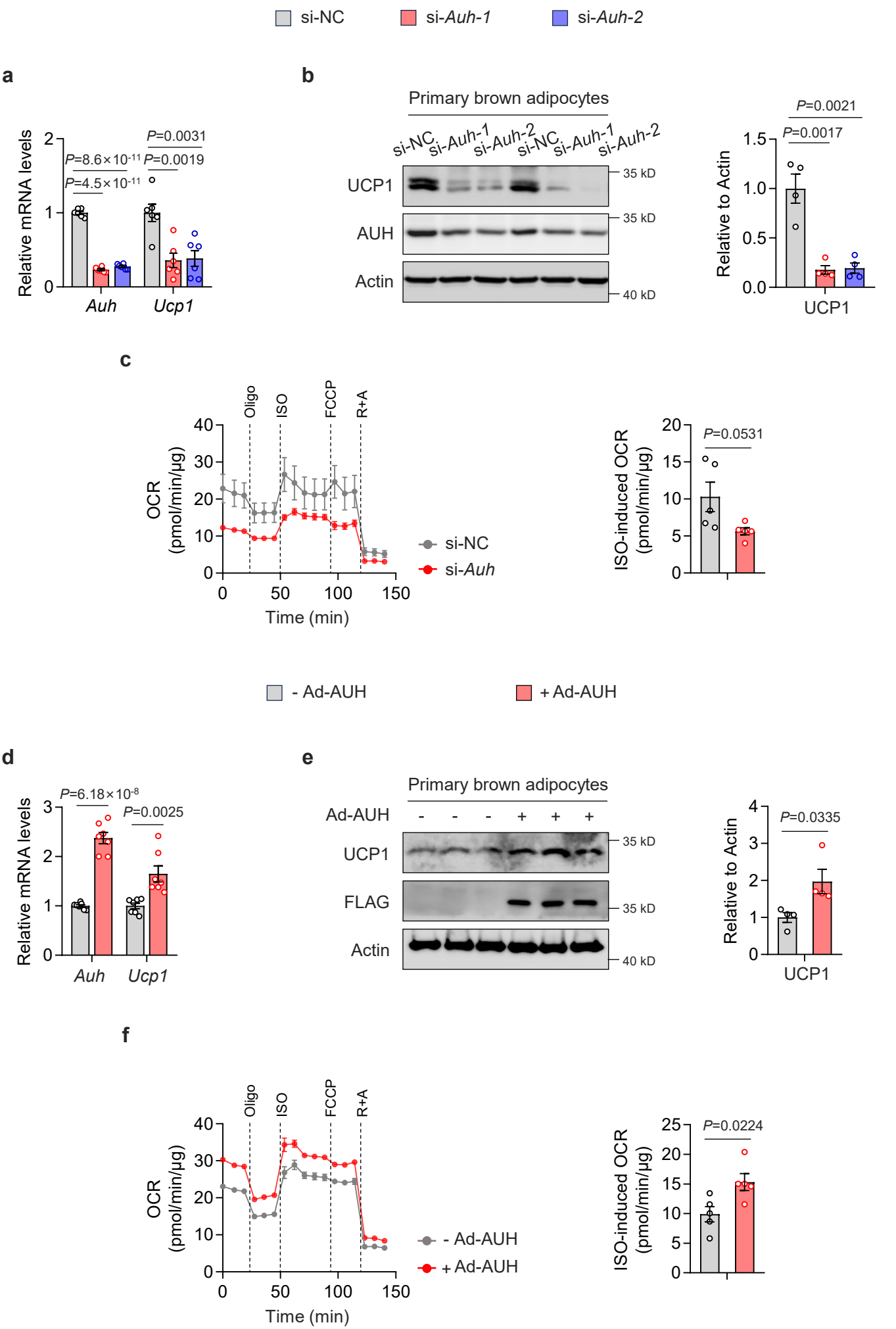
si-NC
si-Auh-1
si-Auh-2
a
Relative mRNA levels
P=8.6×10-11
P=4.5×10-11
P=0.0031
P=0.0019
Auh
Ucp1
b
Primary brown adipocytes
si-NC
si-Auh-1
si-Auh-2
si-NC
si-Auh-1
si-Auh-2
UCP1
AUH
Actin
35 kD
35 kD
40 kD
P=0.0021
P=0.0017
Relative to Actin
UCP1
c
Oligo
ISO
FCCP
R+A
OCR (pmol/min/μg)
Time (min)
si-NC
si-Auh
P=0.0531
ISO-induced OCR (pmol/min/μg)
- Ad-AUH
+ Ad-AUH
d
P=6.18×10-8
P=0.0025
Relative mRNA levels
Auh
Ucp1
e
Primary brown adipocytes
Ad-AUH
UCP1
FLAG
Actin
35 kD
35 kD
40 kD
P=0.0335
Relative to Actin
UCP1
f
Oligo
ISO
FCCP
R+A
OCR (pmol/min/μg)
Time (min)
- Ad-AUH
+ Ad-AUH
P=0.0224
ISO-induced OCR (pmol/min/μg)

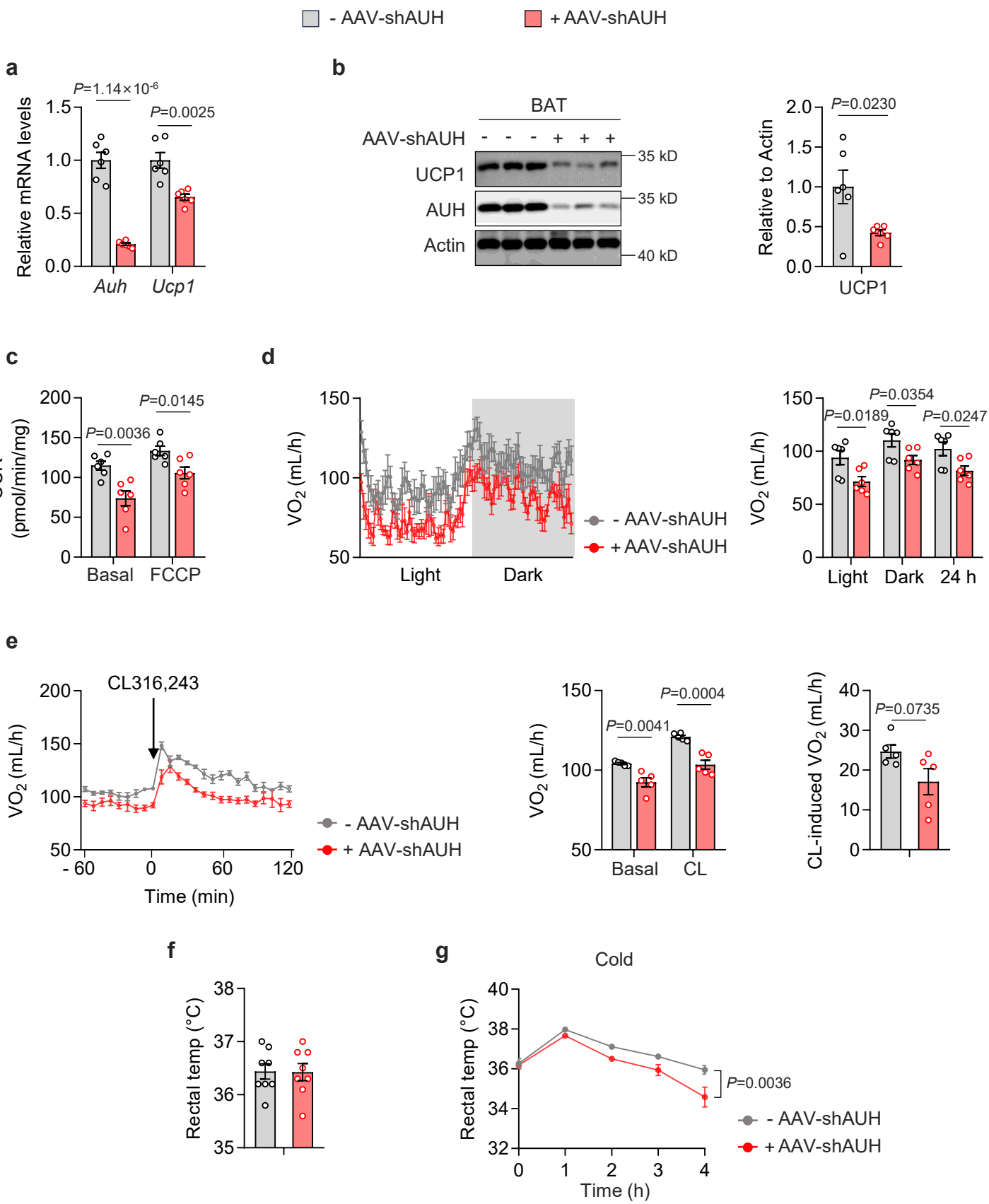
- AAV-shAUH
+ AAV-shAUH
a
P=1.14×10-6
P=0.0025
Relative mRNA levels
Auh
Ucp1
b
BAT
AAV-shAUH
UCP1
AUH
Actin
35 kD
35 kD
40 kD
P=0.0230
Relative to Actin
UCP1
c
P=0.0036
P=0.0145
OCR (pmol/min/mg)
Basal
FCCP
d
VO2 (mL/h)
Light
Dark
- AAV-shAUH
+ AAV-shAUH
P=0.0354
P=0.0189
P=0.0247
Light
Dark
24 h
e
CL316,243
VO2 (mL/h)
Time (min)
- AAV-shAUH
+ AAV-shAUH
P=0.0004
P=0.0041
Basal
CL
P=0.0735
CL-induced VO2 (mL/h)
f
Rectal temp (°C)
g
Cold
Rectal temp (°C)
P=0.0036
Time (h)
- AAV-shAUH
+ AAV-shAUH

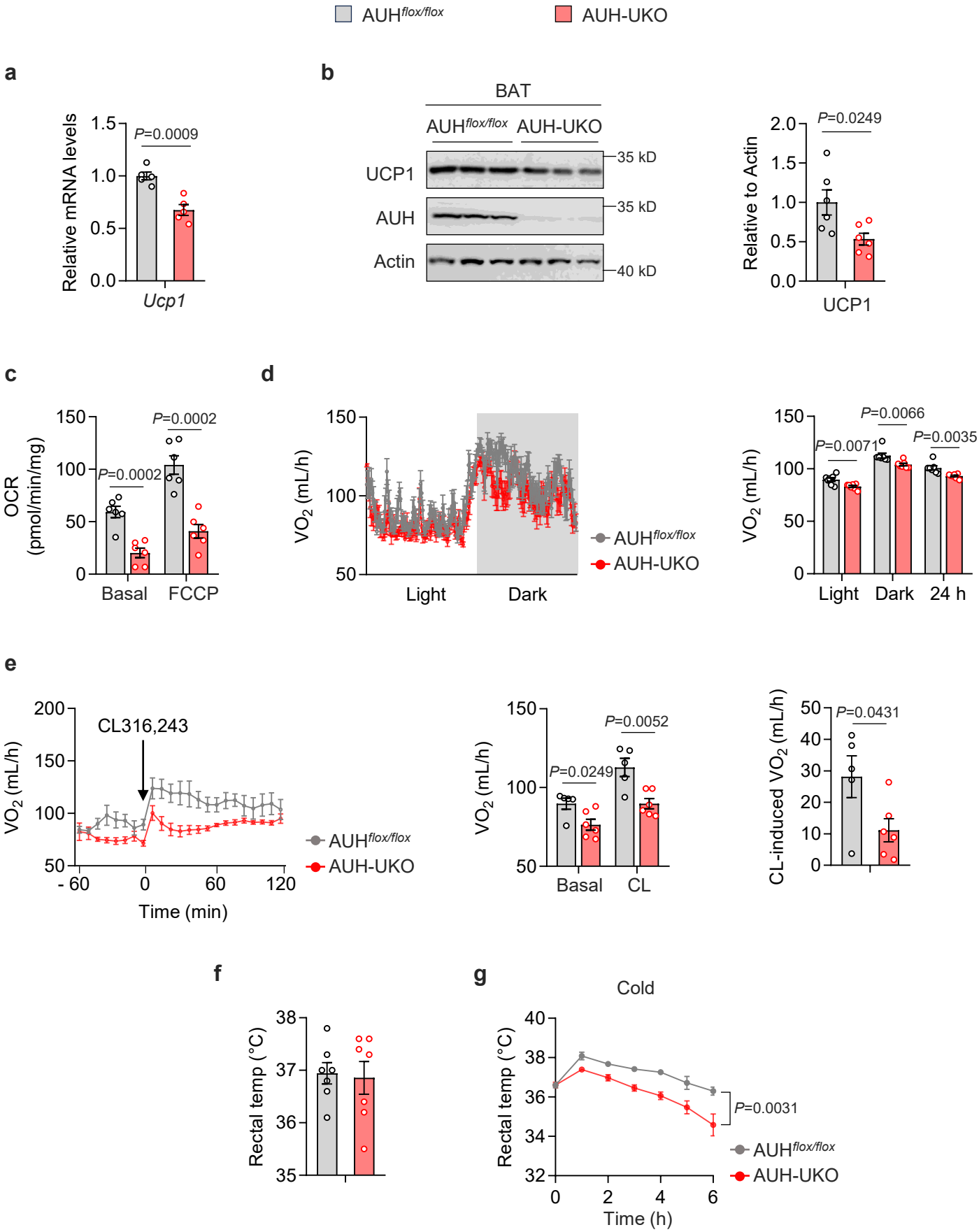
AUH^flox/flox
AUH-UKO
a
Relative mRNA levels
P=0.0009
Ucp1
b
BAT
AUH^flox/flox
AUH-UKO
UCP1
AUH
Actin
35 kD
35 kD
40 kD
Relative to Actin
P=0.0249
UCP1
c
OCR (pmol/min/mg)
P=0.0002
P=0.0002
Basal
FCCP
d
VO2 (mL/h)
Light
Dark
AUH^flox/flox
AUH-UKO
P=0.0071
P=0.0066
P=0.0035
Light
Dark
24 h
e
CL316,243
VO2 (mL/h)
Time (min)
AUH^flox/flox
AUH-UKO
P=0.0249
P=0.0052
Basal
CL
CL-induced VO2 (mL/h)
P=0.0431
f
Rectal temp (°C)
g
Cold
Rectal temp (°C)
P=0.0031
Time (h)
AUH^flox/flox
AUH-UKO

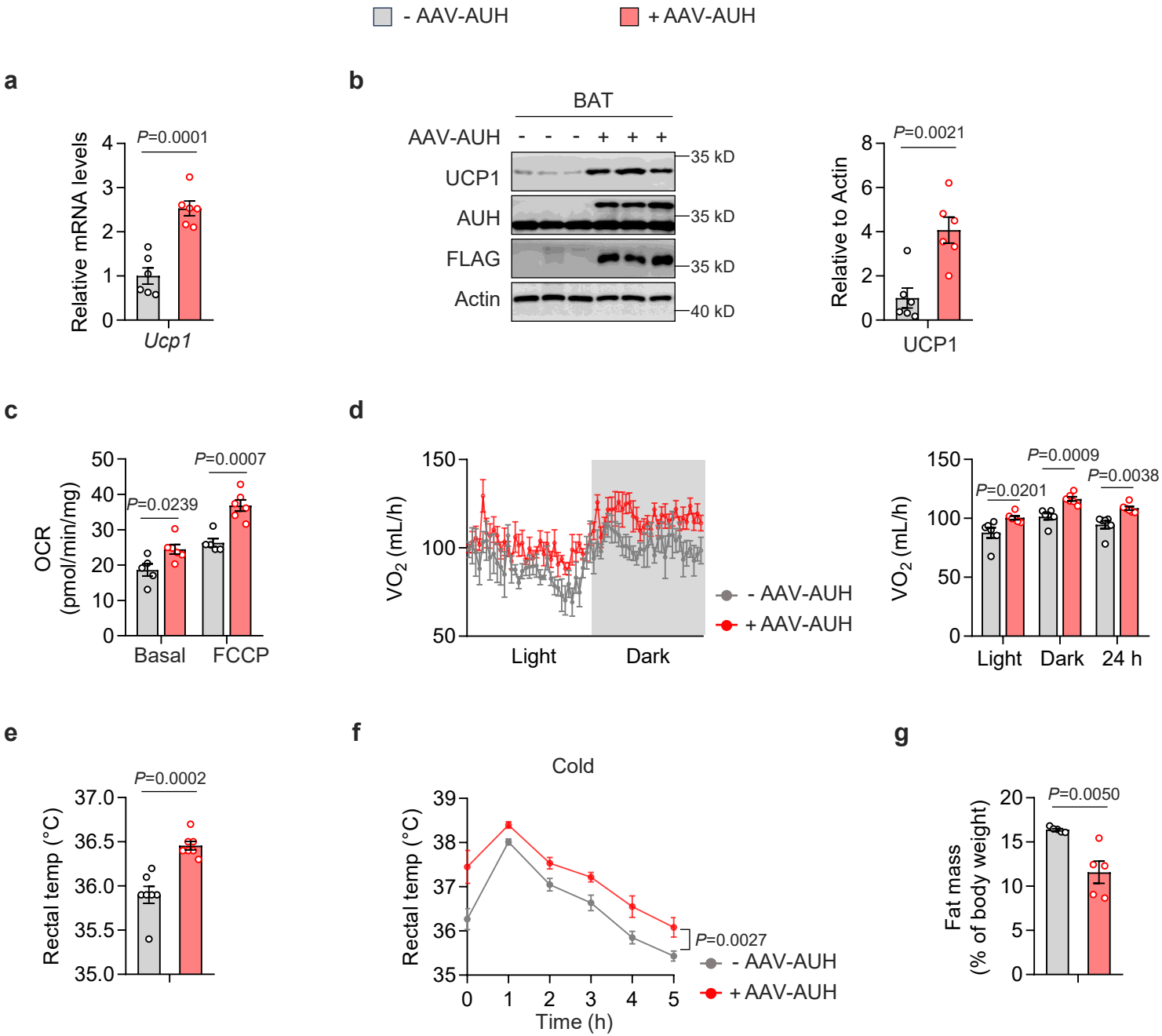
- AAV-AUH
+ AAV-AUH
a
Relative mRNA levels
P=0.0001
Ucp1
b
BAT
AAV-AUH - - - + + +
UCP1
AUH
FLAG
Actin
35 kD
35 kD
35 kD
40 kD
Relative to Actin
P=0.0021
UCP1
c
OCR (pmol/min/mg)
P=0.0239
P=0.0007
Basal
FCCP
d
VO2 (mL/h)
Light
Dark
- AAV-AUH
+ AAV-AUH
P=0.0201
P=0.0009
P=0.0038
Light
Dark
24 h
e
Rectal temp (°C)
P=0.0002
f
Cold
Rectal temp (°C)
P=0.0027
Time (h)
- AAV-AUH
+ AAV-AUH
g
Fat mass (% of body weight)
P=0.0050

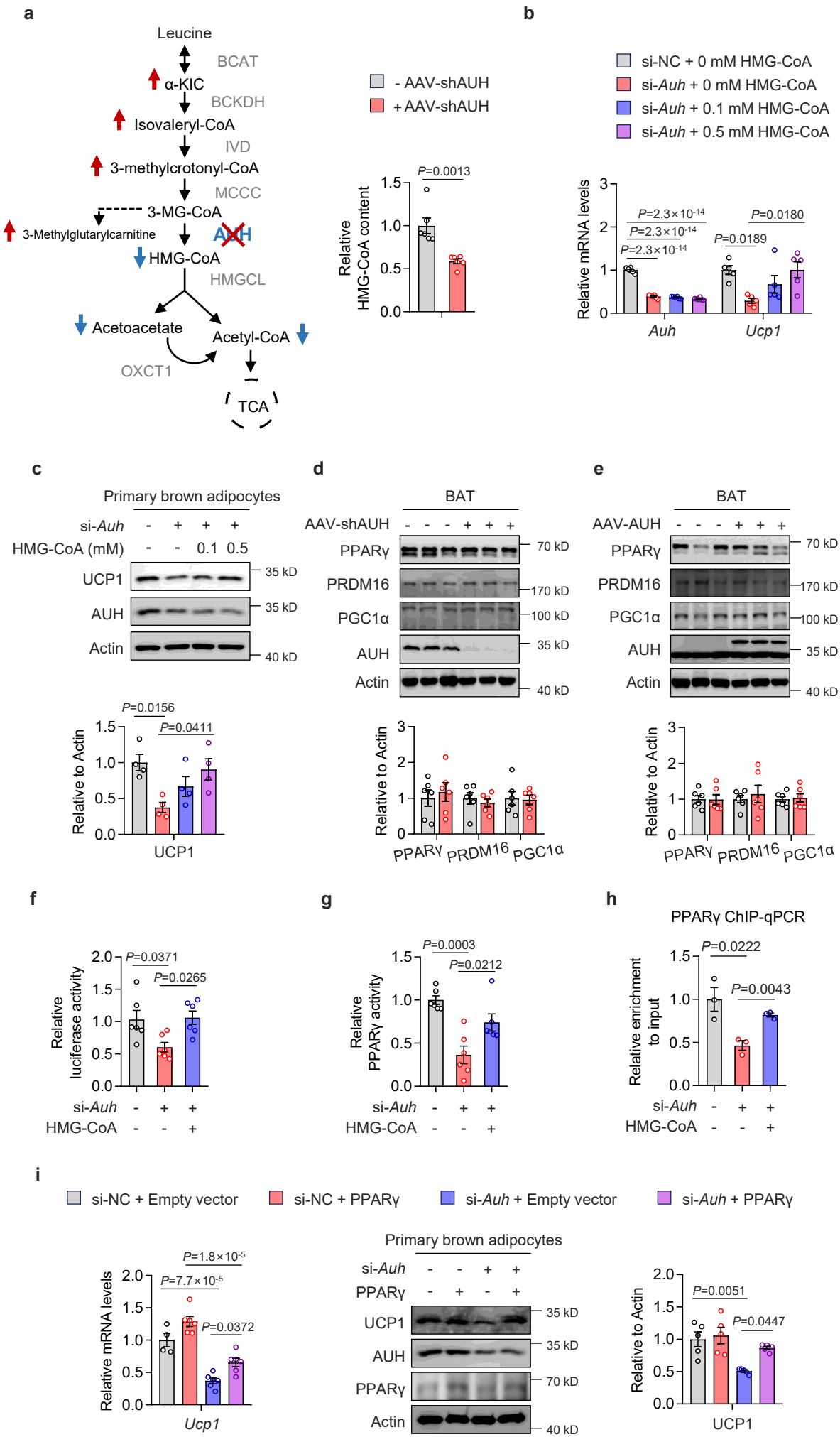
a
Leucine
BCAT
α-KIC
BCKDH
Isovaleryl-CoA
IVD
3-methylcrotonyl-CoA
MCCC
3-MG-CoA
3-Methylglutarylcarnitine
AUH
HMG-CoA
HMGCL
Acetoacetate
Acetyl-CoA
OXCT1
TCA
- AAV-shAUH
+ AAV-shAUH
Relative HMG-CoA content
P=0.0013
b
si-NC + 0 mM HMG-CoA
si-Auh + 0 mM HMG-CoA
si-Auh + 0.1 mM HMG-CoA
si-Auh + 0.5 mM HMG-CoA
Relative mRNA levels
P=2.3×10-14
P=2.3×10-14
P=2.3×10-14
P=0.0189
P=0.0180
Auh
Ucp1
c
Primary brown adipocytes
si-Auh - + + +
HMG-CoA (mM) - - 0.1 0.5
UCP1
AUH
Actin
35 kD
35 kD
40 kD
Relative to Actin
P=0.0156
P=0.0411
UCP1
d
BAT
AAV-shAUH - - - + + +
PPARγ
PRDM16
PGC1α
AUH
Actin
70 kD
170 kD
100 kD
35 kD
40 kD
Relative to Actin
PPARγ PRDM16 PGC1α
e
BAT
AAV-AUH - - - + + +
PPARγ
PRDM16
PGC1α
AUH
Actin
70 kD
170 kD
100 kD
35 kD
40 kD
Relative to Actin
PPARγ PRDM16 PGC1α
f
Relative luciferase activity
P=0.0371
P=0.0265
si-Auh - + +
HMG-CoA - - +
g
Relative PPARγ activity
P=0.0003
P=0.0212
si-Auh - + +
HMG-CoA - - +
h
PPARγ ChIP-qPCR
Relative enrichment to input
P=0.0222
P=0.0043
si-Auh - + +
HMG-CoA - - +
i
si-NC + Empty vector
si-NC + PPARγ
si-Auh + Empty vector
si-Auh + PPARγ
Relative mRNA levels
P=1.8×10-5
P=7.7×10-5
P=0.0372
Ucp1
Primary brown adipocytes
si-Auh - - + +
PPARγ - + - +
UCP1
AUH
PPARγ
Actin
35 kD
35 kD
70 kD
40 kD
Relative to Actin
P=0.0051
P=0.0447
UCP1

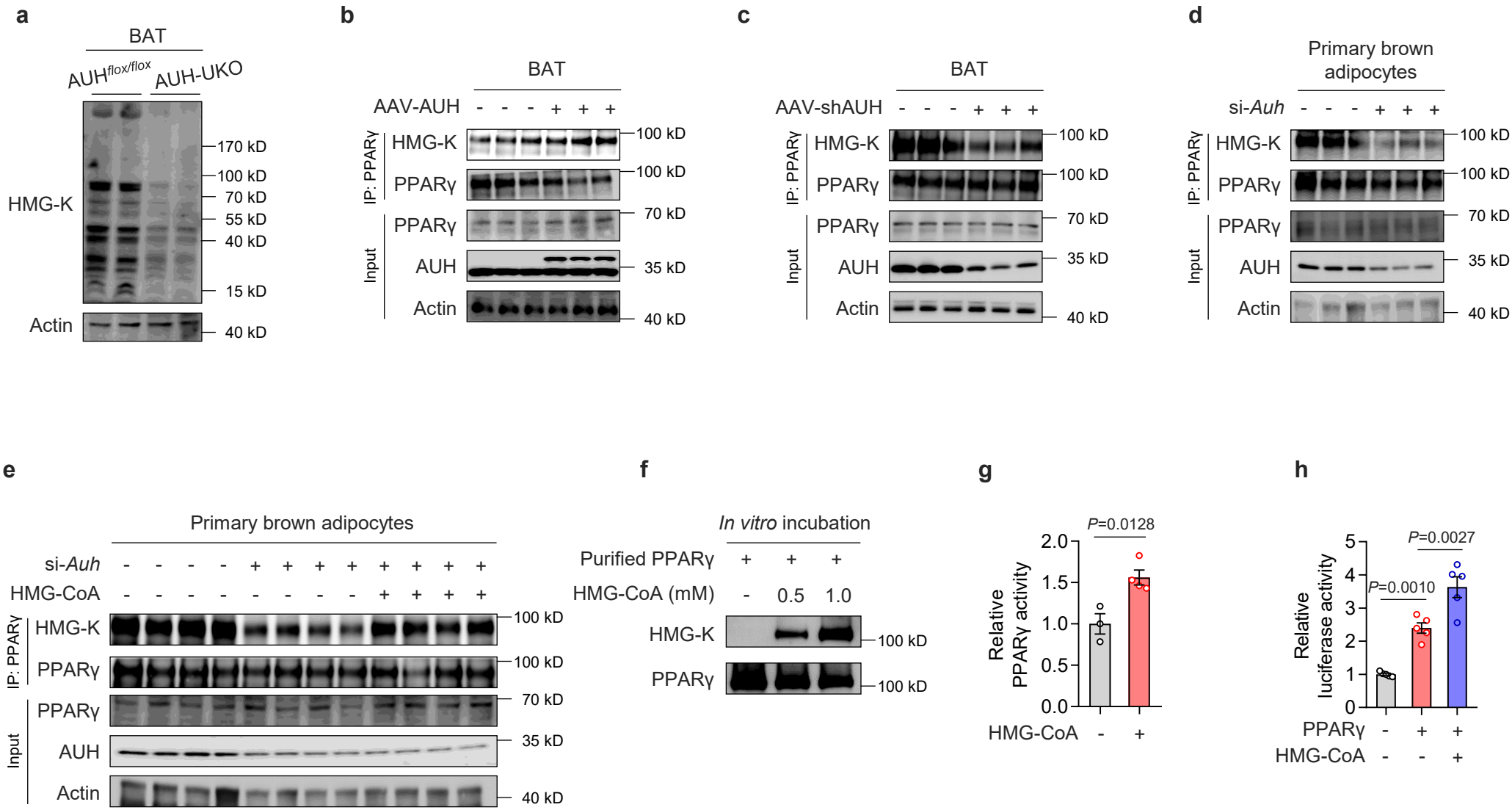
a
BAT
AUH^flox/flox
AUH-UKO
HMG-K
170 kD
100 kD
70 kD
55 kD
40 kD
15 kD
Actin
40 kD
b
BAT
AAV-AUH - - - + + +
IP: PPARγ
HMG-K
100 kD
PPARγ
100 kD
Input
PPARγ
70 kD
AUH
35 kD
Actin
40 kD
c
BAT
AAV-shAUH - - - + + +
IP: PPARγ
HMG-K
100 kD
PPARγ
100 kD
Input
PPARγ
70 kD
AUH
35 kD
Actin
40 kD
d
Primary brown adipocytes
si-Auh - - - + + +
IP: PPARγ
HMG-K
100 kD
PPARγ
100 kD
Input
PPARγ
70 kD
AUH
35 kD
Actin
40 kD
e
Primary brown adipocytes
si-Auh - - - - + + + + + + + +
HMG-CoA - - - - - - - - + + + +
IP: PPARγ
HMG-K
100 kD
PPARγ
100 kD
Input
PPARγ
70 kD
AUH
35 kD
Actin
40 kD
f
In vitro incubation
Purified PPARγ + + +
HMG-CoA (mM) - 0.5 1.0
HMG-K
100 kD
PPARγ
100 kD
g
P=0.0128
Relative PPARγ activity
2.0
1.5
1.0
0.5
0.0
HMG-CoA - +
h
P=0.0027
P=0.0010
Relative luciferase activity
5
4
3
2
1
0
PPARγ - + +
HMG-CoA - - +

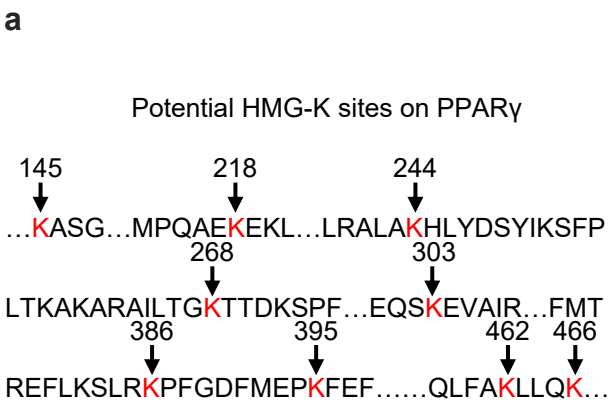
a
Potential HMG-K sites on PPARγ
145
218
244
…KASG…MPQAEKEKL…LRALAKHLYDSYIKSFP
268
303
LTKAKARAILTGKTTDKSPF…EQSKEVAIR…FMT
386
395
462
466
REFLKSLRKPFGDFMEPKFEF……QLFAKLLQK…

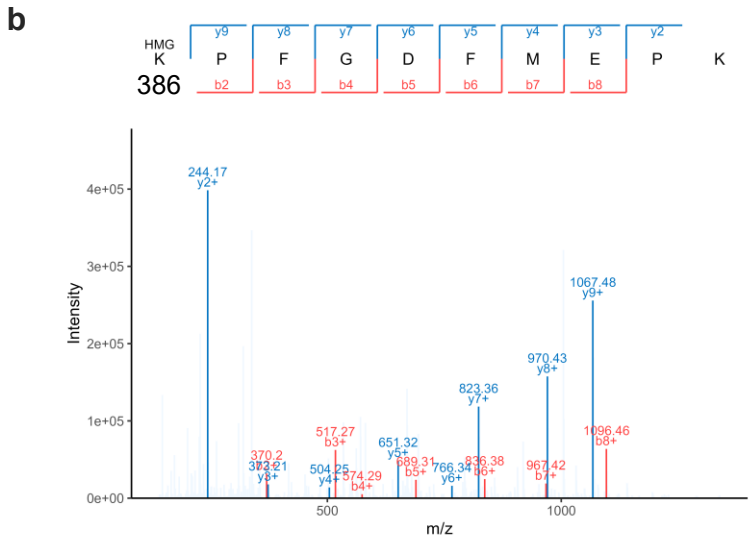
b
HMG
K
386
P F G D F M E P K
y9 y8 y7 y6 y5 y4 y3 y2
b2 b3 b4 b5 b6 b7 b8
Intensity
m/z
244.17 y2+
1067.48 y9+
970.43 y8+
823.36 y7+
1096.46 b8+
517.27 b3+
651.32 y5+
504.25 y4+
574.29 b4+
766.34 y6+
967.42 b7+

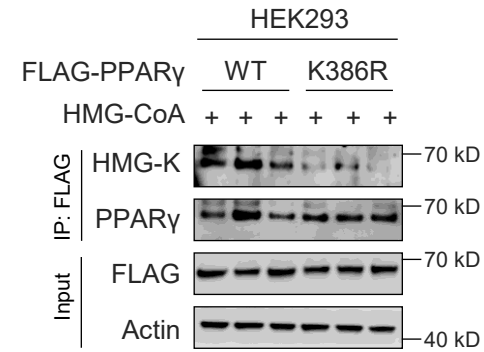
c
HEK293
FLAG-PPARγ
WT
K386R
HMG-CoA
IP: FLAG
HMG-K
PPARγ
Input
FLAG
Actin
70 kD
70 kD
70 kD
40 kD

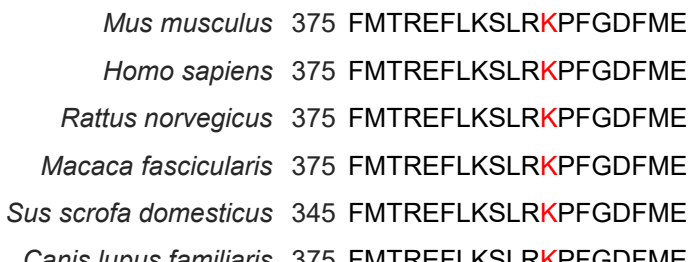
d
Mus musculus 375 FMTREFLKSLRKPFGDFME
Homo sapiens 375 FMTREFLKSLRKPFGDFME
Rattus norvegicus 375 FMTREFLKSLRKPFGDFME
Macaca fascicularis 375 FMTREFLKSLRKPFGDFME
Sus scrofa domesticus 345 FMTREFLKSLRKPFGDFME
Canis lupus familiaris 375 FMTREFLKSLRKPFGDFME
Gallus gallus 345 FMTREFLKSLRKPFCDFME

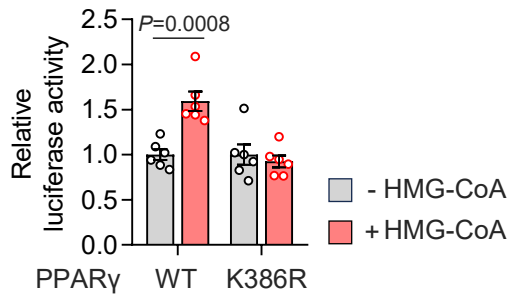
e
Relative luciferase activity
P=0.0008
- HMG-CoA
+ HMG-CoA
PPARγ WT K386R

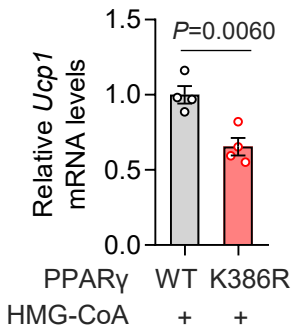
f
Relative Ucp1 mRNA levels
P=0.0060
PPARγ WT K386R
HMG-CoA + +

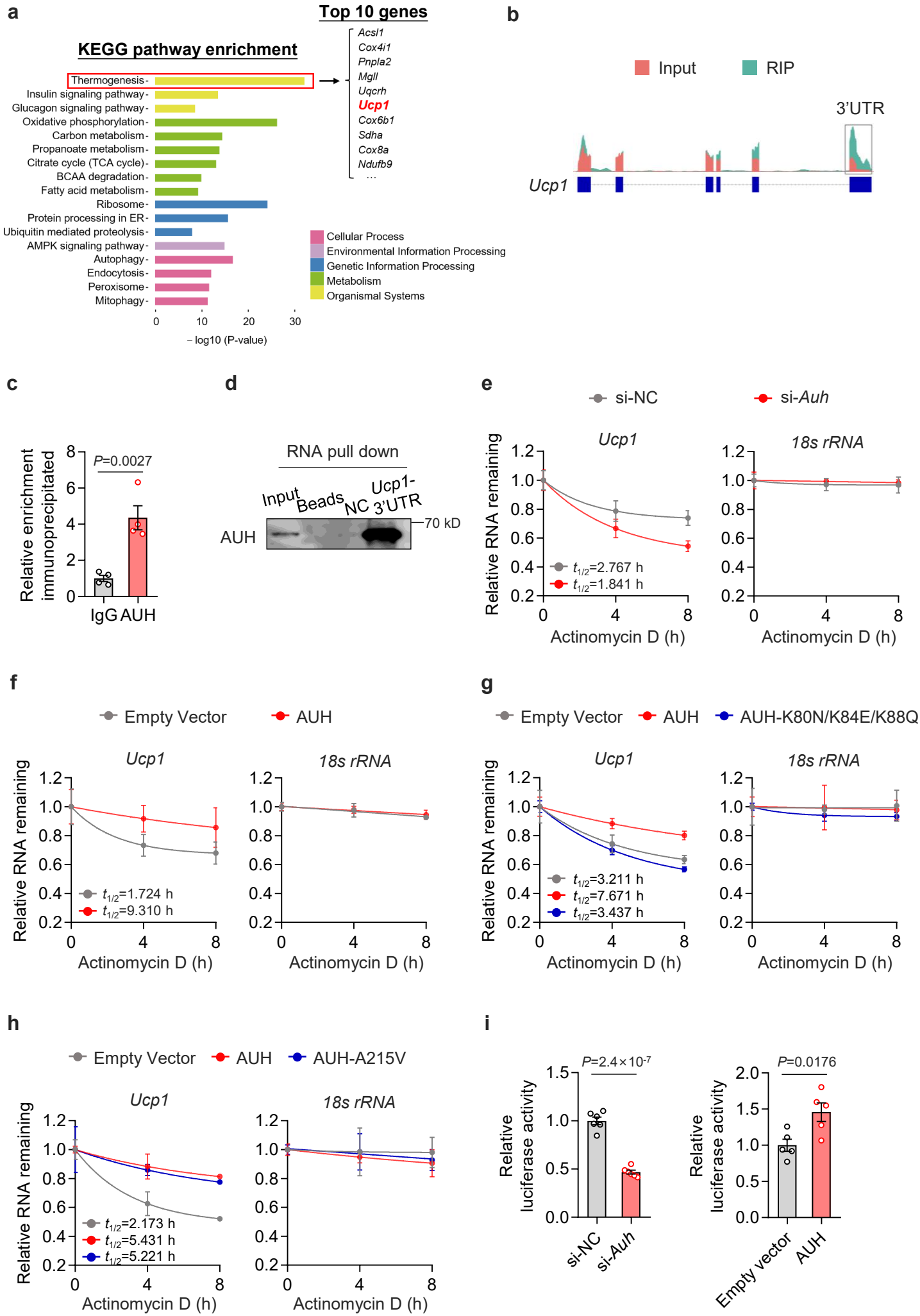
a
KEGG pathway enrichment
Top 10 genes
Thermogenesis
Insulin signaling pathway
Glucagon signaling pathway
Oxidative phosphorylation
Carbon metabolism
Propanoate metabolism
Citrate cycle (TCA cycle)
BCAA degradation
Fatty acid metabolism
Ribosome
Protein processing in ER
Ubiquitin mediated proteolysis
AMPK signaling pathway
Autophagy
Endocytosis
Peroxisome
Mitophagy
Acsl1
Cox4i1
Pnpla2
Mgll
Uqcrh
Ucp1
Cox6b1
Sdha
Cox8a
Ndufb9
Cellular Process
Environmental Information Processing
Genetic Information Processing
Metabolism
Organismal Systems
– log10 (P-value)
b
Input
RIP
3'UTR
Ucp1
c
Relative enrichment immunoprecipitated
P=0.0027
IgG
AUH
d
RNA pull down
Input
Beads
NC
Ucp1-3'UTR
AUH
70 kD
e
si-NC
si-Auh
Ucp1
18s rRNA
Relative RNA remaining
t1/2=2.767 h
t1/2=1.841 h
Actinomycin D (h)
f
Empty Vector
AUH
Ucp1
18s rRNA
Relative RNA remaining
t1/2=1.724 h
t1/2=9.310 h
Actinomycin D (h)
g
Empty Vector
AUH
AUH-K80N/K84E/K88Q
Ucp1
18s rRNA
Relative RNA remaining
t1/2=3.211 h
t1/2=7.671 h
t1/2=3.437 h
Actinomycin D (h)
h
Empty Vector
AUH
AUH-A215V
Ucp1
18s rRNA
Relative RNA remaining
t1/2=2.173 h
t1/2=5.431 h
t1/2=5.221 h
Actinomycin D (h)
i
Relative luciferase activity
P=2.4×10-7
si-NC
si-Auh
P=0.0176
Empty vector
AUH

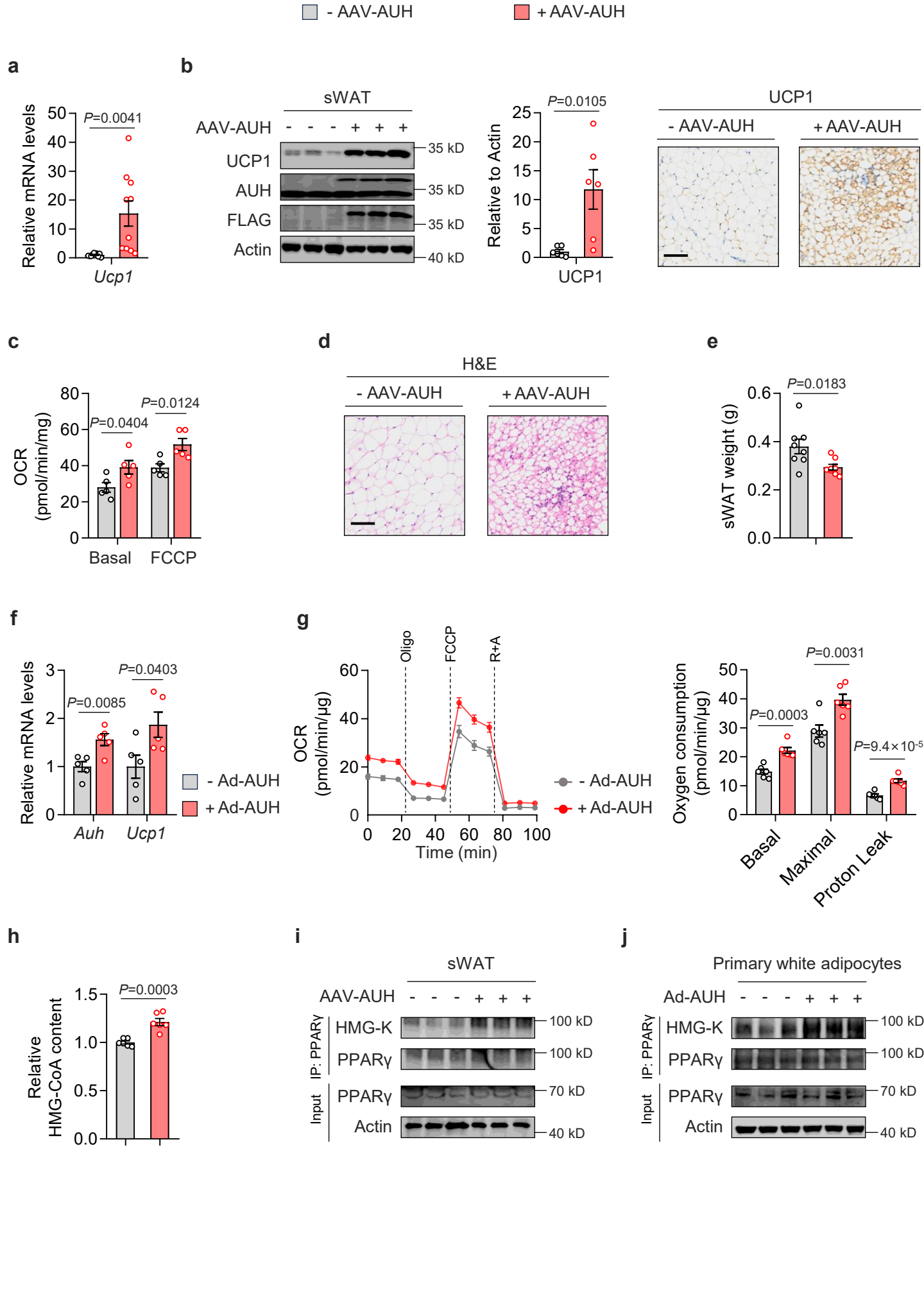
- AAV-AUH
+ AAV-AUH
a
Relative mRNA levels
P=0.0041
Ucp1
b
sWAT
AAV-AUH
UCP1
AUH
FLAG
Actin
35 kD
35 kD
35 kD
40 kD
Relative to Actin
P=0.0105
UCP1
UCP1
- AAV-AUH
+ AAV-AUH
c
OCR (pmol/min/mg)
P=0.0404
P=0.0124
Basal
FCCP
d
H&E
- AAV-AUH
+ AAV-AUH
e
sWAT weight (g)
P=0.0183
f
Relative mRNA levels
P=0.0085
P=0.0403
Auh
Ucp1
- Ad-AUH
+ Ad-AUH
g
OCR (pmol/min/μg)
Oligo
FCCP
R+A
Time (min)
- Ad-AUH
+ Ad-AUH
Oxygen consumption (pmol/min/μg)
P=0.0003
P=0.0031
P=9.4×10-5
Basal
Maximal
Proton Leak
h
Relative HMG-CoA content
P=0.0003
i
sWAT
AAV-AUH
IP: PPARγ
HMG-K
PPARγ
Input
PPARγ
Actin
100 kD
100 kD
70 kD
40 kD
j
Primary white adipocytes
Ad-AUH
IP: PPARγ
HMG-K
PPARγ
Input
PPARγ
Actin
100 kD
100 kD
70 kD
40 kD

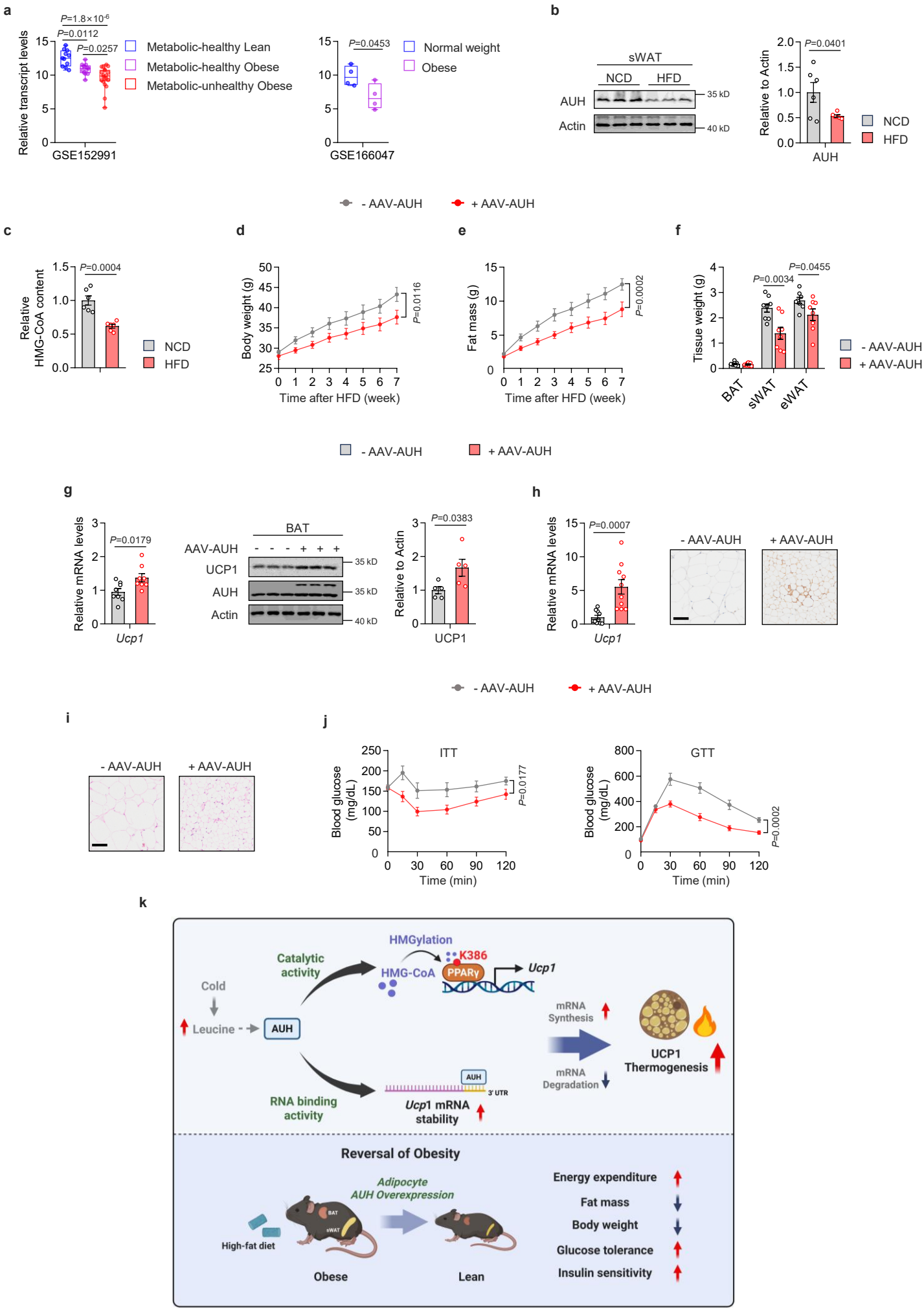
a
P=1.8×10-6
P=0.0112
P=0.0257
Relative transcript levels
Metabolic-healthy Lean
Metabolic-healthy Obese
Metabolic-unhealthy Obese
GSE152991
P=0.0453
Normal weight
Obese
GSE166047
b
sWAT
NCD
HFD
AUH
Actin
35 kD
40 kD
Relative to Actin
P=0.0401
NCD
HFD
AUH
- AAV-AUH
+ AAV-AUH
c
Relative HMG-CoA content
P=0.0004
NCD
HFD
d
Body weight (g)
P=0.0116
Time after HFD (week)
e
Fat mass (g)
P=0.0002
Time after HFD (week)
f
Tissue weight (g)
P=0.0034
P=0.0455
BAT
sWAT
eWAT
- AAV-AUH
+ AAV-AUH
g
Relative mRNA levels
P=0.0179
Ucp1
BAT
AAV-AUH
UCP1
AUH
Actin
35 kD
35 kD
40 kD
Relative to Actin
P=0.0383
UCP1
h
Relative mRNA levels
P=0.0007
Ucp1
- AAV-AUH
+ AAV-AUH
i
- AAV-AUH
+ AAV-AUH
j
ITT
Blood glucose (mg/dL)
P=0.0177
Time (min)
GTT
Blood glucose (mg/dL)
P=0.0002
Time (min)
k
Cold
Leucine
AUH
Catalytic activity
HMGylation
K386
HMG-CoA
PPARγ
Ucp1
RNA binding activity
AUH
3' UTR
Ucp1 mRNA stability
mRNA Synthesis
mRNA Degradation
UCP1 Thermogenesis
Reversal of Obesity
Adipocyte AUH Overexpression
High-fat diet
BAT
sWAT
Obese
Lean
Energy expenditure
Fat mass
Body weight
Glucose tolerance
Insulin sensitivity